Article

A parabrachial hub for need-state control of enduring pain

https://doi.org/10.1038/s41586-025-09602-x

Received: 26 January 2024

Accepted: 8 September 2025

Published online: 8 October 2025

Open access

Check for updates

Nitsan Goldstein[1,12], Amadeus Maes[2,12], Heather N. Allen[3,4,5], Tyler S. Nelson[3,4,5], Kayla A. Kruger[1], Morgan Kindel[1], Albert T. M. Yeung[1], Nicholas K. Smith[1], Jamie R. E. Carty[1], Lavinia Boccia[1], Niklas Blank[6,7], Emily Lo[1], Rachael E. Villari[1], Ella Cho[1], Erin L. Marble[1], Michelle Awh[1], Yasmina Dumiaty[8], Melissa J. Chee[8], Rajesh Khanna[3], Christoph A. Thaiss[6,7], Bradley K. Taylor[4,5]✉, Ann Kennedy[2]✉ & J. Nicholas Betley[1,9,10,11]✉

Long-term sustained pain following acute physical injury is a prominent feature of chronic pain conditions[1]. Populations of neurons that rapidly respond to noxious stimuli or tissue damage have been identified in the spinal cord and several nuclei in the brain[2–4]. Understanding the central mechanisms that signal ongoing sustained pain, including after tissue healing, remains a challenge[5]. Here we use spatial transcriptomics, neural manipulations, activity recordings and computational modelling to demonstrate that activity in an ensemble of anatomically and molecularly diverse parabrachial neurons that express the neuropeptide Y (NPY) receptor Y1 (Y1R neurons) is increased following injury and predicts functional coping behaviour. Hunger, thirst or predator cues suppressed sustained pain, regardless of the injury type, by inhibiting parabrachial Y1R neurons via the release of NPY. Together, our results demonstrate an endogenous analgesic hub at pain-responsive parabrachial Y1R neurons.

Despite progress in understanding neural pathways that process the sensory and emotional dimensions of acute pain[6,7], the brain network that is engaged in long-term pain states has remained unidentified[8]. Populations of neurons that are activated during transient noxious stimuli have been identified throughout the peripheral and central nervous systems[4,9–15]. Altered spinal circuitry following injury is well documented and, at least in part, underlies transitions to chronic pain[2,16,17]. Ascending spinal pathways project to neural nodes that are likely to code and relay the multimodal sensory and affective dimensions of long-term pain. Identification of neurons that respond specifically in the pain state, and not just to transient noxious stimuli, would serve as a foundation for understanding how changes in neural activity lead to maladaptive, chronic pain[18,19].

Consistent changes in neural activity during persistent pain are not clearly discernible from human imaging studies[8]. We considered how state-tuned neurons in the brain could be identified. We focused on the lateral parabrachial nucleus (lPBN), a major entry point of sensory information from the periphery and the first site of integration of many affective behavioural states. Populations of neurons in the lPBN receive direct input from the dorsal horn of the spinal cord and respond to acute nociceptive stimuli, and prolonged activation of excitatory lPBN neurons can drive a chronic pain-like state[13,20–22]. This strategic location makes the lPBN an efficient site at which pain could be modulated.

Here we identify an ensemble of neurons in the lPBN that is activated during persistent pain. These neurons are distributed across molecularly and anatomically defined subpopulations and are unified by the expression of the NPY receptor Y1 (Y1R). Neural activity monitoring and computational modelling demonstrate that sustained activity in these neurons correlates with lasting pain. We also show that a variety of ethologically relevant need states suppress sustained pain responses and demonstrate that Y1R-expressing neurons are a central hub for the convergence of pain information with endogenous analgesic circuits that are activated by competing need states[23]. This cellular target provides a neurophysiological proxy for monitoring sustained pain and a potential intervention point to reduce pain in pathological conditions.

Y1R neurons affect sustained pain-like responses

We performed spatial transcriptomics on mouse parabrachial nucleus (PBN) tissue following formalin paw injection with a goal of identifying populations of PBN neurons that are activated by persistent noxious stimulation. Neighbourhood analysis identified spatial niches that were used to restrict further analyses to the medial, dorsal lateral, ventral lateral and external lateral subdivisions of the PBN (Fig. 1a). We first examined how cell types are distributed molecularly and spatially within the PBN. We identified 24 clusters of cells (Extended Data Fig. 1a), including many that were enriched in glial markers (Extended Data Fig. 1b–e and

[1]Department of Biology, University of Pennsylvania, Philadelphia, PA, USA. [2]Department of Neuroscience, The Scripps Research Institute, La Jolla, CA, USA. [3]Department of Pharmacology and Therapeutics, McKnight Brain Institute, Center for Advanced Pain Therapeutics and Research (CAPToR), University of Florida College of Medicine, Gainesville, FL, USA. [4]Department of Anesthesiology and Perioperative Medicine, University of Pittsburgh School of Medicine, Pittsburgh, PA, USA. [5]Pittsburgh Center for Pain Research, Pittsburgh Project to End Opioid Misuse, University of Pittsburgh School of Medicine, Pittsburgh, PA, USA. [6]Department of Pathology, Stanford University, Stanford, CA, USA. [7]Arc Institute, Palo Alto, CA, USA. [8]Department of Neuroscience, Carleton University, Ottawa, Ontario, Canada. [9]Institute for Obesity, Diabetes, and Metabolism, Perelman School of Medicine, University of Pennsylvania, Philadelphia, PA, USA. [10]Department of Neuroscience, Perelman School of Medicine, University of Pennsylvania, Philadelphia, PA, USA. [11]BrainBodyBiome Center, University of Pennsylvania, Philadelphia, PA, USA. [12]These authors contributed equally: Nitsan Goldstein, Amadeus Maes. ✉e-mail: bkt@pitt.edu; akennedy@scripps.edu; jnbetley@sas.upenn.edu

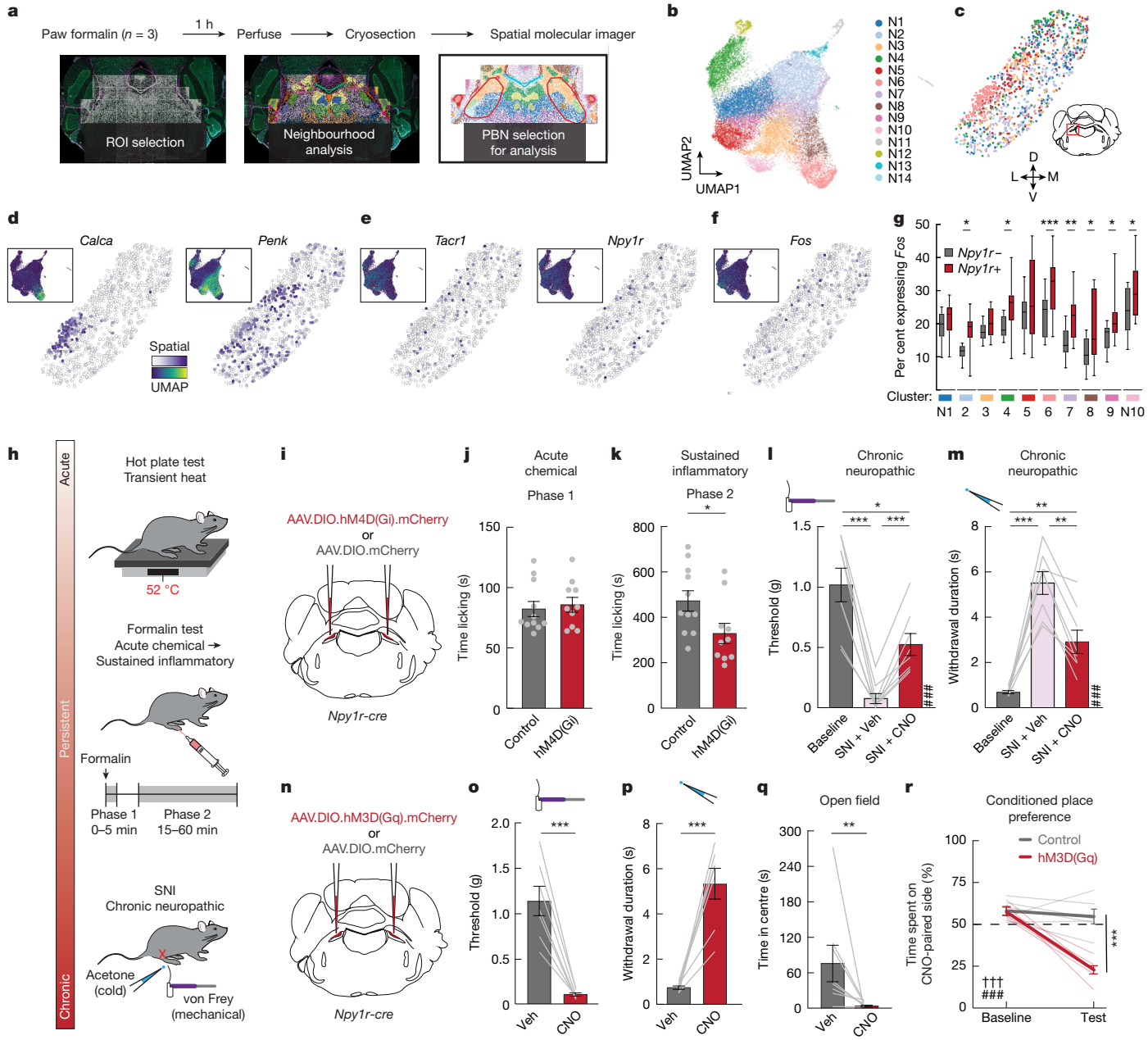

Fig. 1 | lPBN Y1 receptor-expressing neurons influence sustained and chronic pain. a, Mice were injected with formalin in the hindpaw before sample collection. PBN sections were analysed using a spatial molecular imager (CosMx). $n = 3$ mice, 4 sections each. ROI, region of interest. **b**, Uniform manifold approximation and projection (UMAP) embedding of PBN neuron clusters. **c**, Representative spatial map of molecularly defined clusters. D, dorsal; L, lateral; M, medial; V, ventral. **d**, UMAP embeddings and representative spatial maps showing normalized expression levels of *Calca* and *Penk*. UMAP scale maximum: *Calca*, 3.7; *Penk*, 4.5. Spatial scale maximum: *Calca*, 3.3; *Penk*, 4.2. **e**, Normalized expression levels of *Tacr1* and *Npy1r*. UMAP scale maximum: *Tacr1*, 1.9; *Npy1r*, 2.25. Spatial scale maximum: *Tacr1*, 1.4; *Npy1r*, 1.5. **f**, Normalized expression levels of *Fos*. UMAP scale maximum: 2.55. Spatial scale maximum: 1.75. **g**, Percentage of *Npy1r*-expressing and non-expressing cells co-expressing *Fos*. Box plots show the median (centre line), 25th–75th percentiles (box) and 5th–95th percentiles (whiskers) ($n = 6$ to 12 sections per group; two-way ANOVA, main effect of group $P < 0.001$). **h**, Assays used to assess pain behaviour. **i**, Strategy to inhibit lPBN Y1R neurons. **j**,**k**, Time licking paw after formalin during phase 1 (**j**) and phase 2 (**k**) in control or with Y1R neuron inhibition ($n = 11$ control, $n = 10$ hm4D(Gi) mice; unpaired two-sided t-test, not significant (**j**), $P = 0.0352$ (k)). **l**,**m**, Withdrawal threshold (mechanical; **l**) or duration (acetone; **m**) in hM4D (Gi)-expressing mice before SNI and after SNI with a vehicle (Veh) or clozapine-*N*-oxide (CNO) injection ($n = 8$ mice; one-way ANOVA, $P < 0.001$). **n**, Strategy to activate lPBN Y1R neurons. **o**,**p**, Withdrawal threshold (mechanical; **o**) or duration (acetone; **p**) in hM3D(Gq)-expressing mice after a vehicle or CNO injection ($n = 7$ mice; paired two-sided t-test, $P = 0.0005$). **q**, Time spent in the centre of an open field ($n = 8$ mice; two-sided Wilcoxon matched pairs signed-rank test, $P = 0.0078$). **r**, Percentage of time spent in the side of a chamber paired with CNO ($n = 6$ control, $n = 7$ hm4D(Gi) mice; two-way ANOVA, main effect of group $P = 0.0002$, group × time interaction $P < 0.001$). Data are mean ± s.e.m. unless noted otherwise. Grey dots and lines represent individual mice. t-test and post hoc comparisons: $^{*}P < 0.05$, $^{**}P < 0.01$, $^{***}P < 0.001$. ANOVA main effect of group: $^{\#}P < 0.05$, $^{\#\#}P < 0.01$, $^{\#\#\#}P < 0.001$. ANOVA interaction: $^{\dagger}P < 0.05$, $^{\dagger\dagger}P < 0.01$, $^{\dagger\dagger\dagger}P < 0.001$.

Supplementary Fig. 1). Analysis of 32,169 cells enriched in neural markers (Extended Data Fig. 1f–h) revealed 14 distinct PBN clusters (Fig. 1b,c, Extended Data Fig. 1i and Supplementary Fig. 1) that largely align with prior analyses of PBN cell types[24–26]. Genes that were known to label neurons previously studied in pain-related behaviours were restricted to a small number of molecularly defined clusters that were also

spatially confined. These included *Penk*-expressing neurons, *Pdyn*-expressing neurons, and *Calca*-expressing neurons, many of which also express *Adcyap1*, *Tac1* and the opioid receptor gene *Oprm1* (Fig. 1d and Extended Data Figs. 1j and 2a). This pattern contrasts with the expression of neuropeptide receptor genes such as *Tacr1* and Y1R (*Npy1r*), which were spatially distributed and found across many molecularly defined clusters (Fig. 1e and Extended Data Fig. 1j). In situ hybridization confirmed our observation that *Npy1r*-expressing neurons (lPBN Y1R neurons) were spatially and molecularly distinct from other previously characterized PBN neuron types (Extended Data Fig. 2c–q).

Immediate early gene (IEG) expression in response to formalin injection was also distributed across clusters, suggesting that PBN neurons that are activated by persistent pain are not transcriptionally or anatomically distinct subpopulations (Fig. 1f and Extended Data Fig. 2b). We found that the IEG *Fos* was enriched in neurons that express *Npy1r* (Fig. 1g). This was intriguing, given our previous finding that NPY signalling in the lPBN can suppress inflammatory pain[27]. Fluorescent labelling of Y1R neurons revealed projections along both the central tegmental tract (amygdala and medial thalamus) and the ventral pathway (hypothalamus), consistent with their anatomical and molecular diversity[24,25] (Supplementary Fig. 2). This distributed organization of lPBN Y1R neurons positions them to receive a wide range of inputs, including nociceptive signals from the spinal cord, and relay information throughout the brain.

To determine the functional role of lPBN Y1R neurons in pain-related behaviour, we performed bidirectional neural activity manipulations in models of acute and chronic pain (Fig. 1h). We used the hot plate assay to test acute thermal nociception, the formalin assay to test acute chemical and sustained inflammatory pain, and the spared nerve injury (SNI) model to test chronic neuropathic pain. von Frey filaments applied to the hind paw were used to evaluate mechanical sensitivity and acetone was used to evaluate cold sensitivity. Chemogenetic inhibition of lPBN Y1R neurons suppressed sustained and chronic behavioural responses to injury without influencing acute responses. Both formalin-induced inflammatory responses and SNI-induced mechanical and cold allodynia were suppressed by chemogenetic inhibition of lPBN Y1R neurons (Fig. 1i,k–m and Supplementary Fig. 3a–f). Responses to transient heat (Supplementary Fig. 3g,h) and acute chemical (Fig. 1j) responses were not modulated by chemogenetic inhibition. Ablating lPBN Y1R neurons also attenuated lasting pain behaviours (Extended Data Fig. 3a–h) without observable effects on locomotion or other aversive or threatening stimuli (Extended Data Fig. 3i–r).

We next explored whether activity in Y1R neurons leads to a pain-like state. To test whether Y1R neurons are sufficient to evoke the sensory and affective responses that follow injury, we expressed the excitatory chemogenetic receptor hM3D(Gq) in lPBN Y1R neurons (Fig. 1n). Activation produced mechanical and cold allodynia as well as spontaneous responses that are often exhibited by animals following injury such as running, jumping and anxiety-like behaviour (Fig. 1o–q and Supplementary Fig. 3i–l). Mice strongly avoided a context that was paired with activation of lPBN Y1R neurons, suggesting that they promote negative affect (Fig. 1r). Together, these results suggest that lPBN Y1R neurons are an essential neural node through which long-term pain information is signalled.

Y1R neurons are activated during sustained pain

We next explored the in vivo calcium dynamics of lPBN Y1R neurons to characterize their activity in persistent pain states. We first monitored neural activity in lPBN Y1R neurons during formalin-induced pain using fibre photometry (Fig. 2a). We observed marked bilateral increases in activity in both phases in which the animal exhibits pain-related behaviour. During these phases, we found rapid fluctuations that correlated with the fine timing of licking bouts as well as slower, sustained increases in activity that occurred during both phases of the response to formalin (Fig. 2b,c and Supplementary Fig. 4a–h). These responses were not purely tactile or motor (Supplementary Fig. 4i–l) and Y1R neurons were not activated by other innately aversive stimuli (trimethylthiazoline (TMT); Supplementary Fig. 4m–q), suggesting that they are selectively activated following painful stimuli.

We quantified the relationship between lPBN neural activity and hindlimb licking after formalin injection by fitting a linear model to recorded population activity. We found that fast changes in Y1R neuron activity were predicted by lick bouts convolved with a fast exponential filter (Fig. 2d). We also determined that there was a residual and sustained increase in neural activity during both phases that persisted when animals were not actively licking (Fig. 2e). Adding a slow, behaviour-independent component to the model significantly improved the fit (Fig. 2e,f). This suggests that Y1R population activity during the formalin assay reflects a combination of fast responses during coping behaviours on top of a slowly shifting baseline that may reflect a persistent pain state.

lPBN Y1R neurons were also sensitized in models of persistent inflammation and neuropathic pain. In vivo Y1R neuron responses to innocuous mechanical and thermal stimuli were significantly enhanced after SNI (Extended Data Fig. 4a–p). To explore potential sources of this enhanced response, we recorded from lPBN Y1R neurons in acute slices one day after injecting mice with complete Freund's adjuvant (CFA) in the paw to evoke persistent inflammation (Extended Data Fig. 4q). CFA significantly increased the frequency and amplitude of spontaneous excitatory post synaptic currents (sEPSCs), indicative of increased excitatory drive onto these neurons (Extended Data Fig. 4r–t). Consistent with the behavioural effects that we observed, activating G_i signalling attenuated spontaneous firing in lPBN Y1R neurons after CFA (Extended Data Fig. 4u,v).

We next interrogated whether the neural dynamics that we observed were unique to the Y1R neurons in the lPBN. We first monitored all non-Y1R neurons in the lPBN (Fig. 2g and Extended Data Fig. 5a–d) and determined that activity in these neurons did not increase significantly after formalin administration. The correlation between neural activity and behaviour was also weaker in non-Y1R neurons than in Y1R neurons (Fig. 2h–l). Notably, Y1R and non-Y1R neurons both responded to acute noxious heat (Supplementary Fig. 5). This is consistent with our recordings from lPBN glutamatergic neurons as well as *Pdyn*- and *Penk*-expressing neurons, none of which exhibited significant slow response components during the second (inflammatory) phase following formalin administration (Extended Data Fig. 5e–p and Supplementary Fig. 6). Thus, although other lPBN populations respond to acute nociceptive stimuli[14,22,28] the population dynamics observed during sustained pain are unique to the Y1R population.

We next investigated what underlies the slow, persistent component of Y1R neuron responses during sustained pain. One possibility is that distinct Y1R neural subpopulations display time-locked, behaviour-associated activity and elevated tonic activity. Alternatively, the same neurons might become tonically active while still responding in bursts during lick bouts. To distinguish between these possibilities, we monitored the activity dynamics of individual lPBN Y1R neurons for 1 h after a formalin injection (Fig. 2m). A correlational analysis revealed several classes of neurons with distinct activity profiles. One class of neurons (accounting for around 40% of lPBN Y1R neurons) was consistently active during lick bouts, whereas calcium fluorescence in a second class (around 16% of lPBN Y1R neurons) increased after formalin injection and remained high for several minutes, independent of specific pain-related behaviours (Fig. 2n–p and Supplementary Fig. 7). These results suggest that the slower component of the Y1R population response is coded by a distinct subset of the Y1R ensemble that are tonically active during sustained pain.

Urgent survival threats act on lPBN Y1R neurons

The expression of Y1R neurons in the lPBN that encode the pain state enables their modulation by NPY. We sought to determine the ability

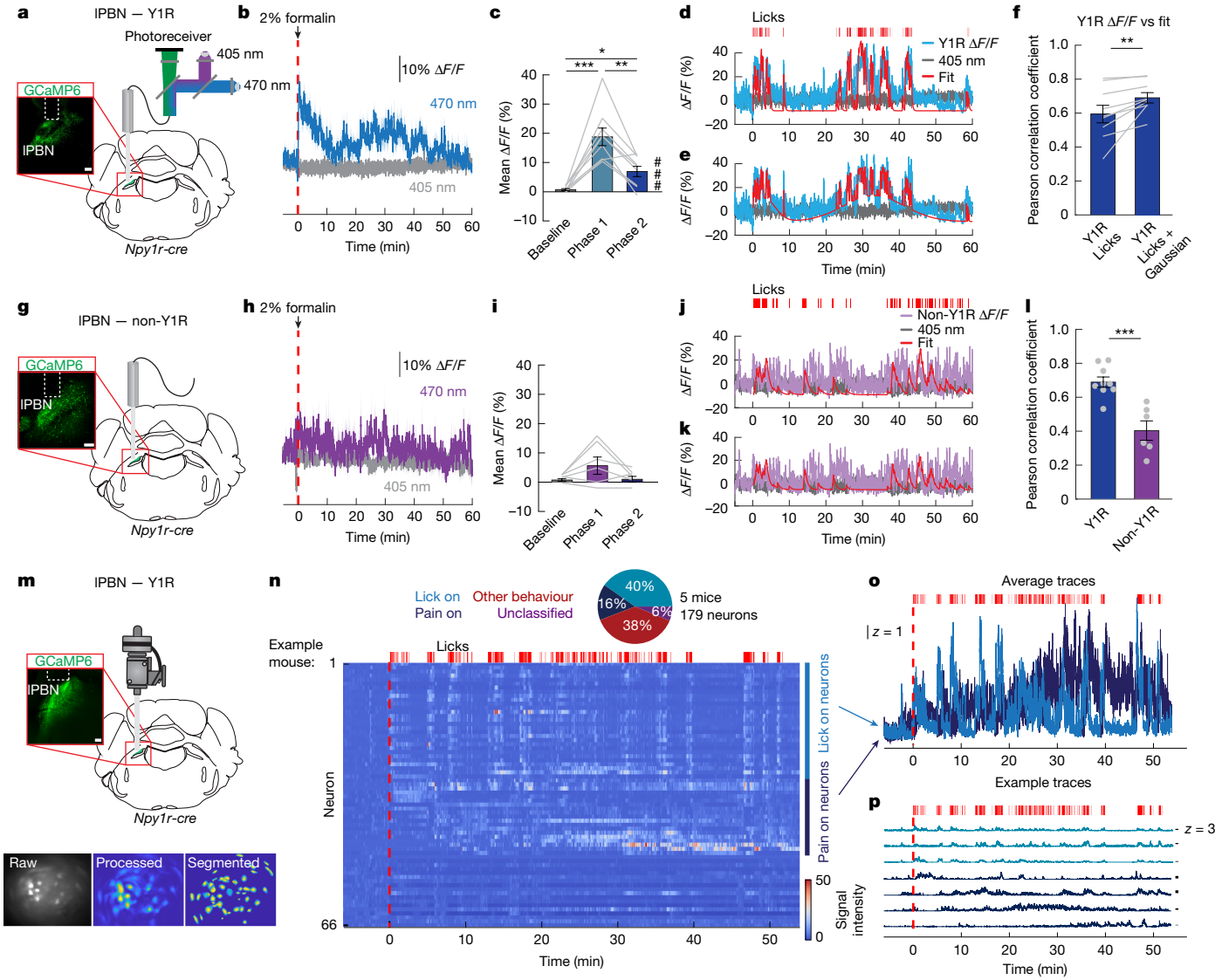

Fig. 2 | Tonic lPBN Y1R neuron activity tracks sustained pain. a, Fibre photometry measurements of lPBN Y1R calcium dynamics. Inset, GCaMP6s expression. Scale bar, 200 µm. **b**, Average Δ*F*/*F* of Y1R neuron GCaMP6s signal after a hind paw formalin injection (dashed red line). Dark lines represent mean and lighter, shaded areas represent s.e.m. **c**, Mean Δ*F*/*F* of Y1R neurons ($n = 9$ mice; repeated measures one-way ANOVA, $P < 0.001$). **d**, Representative trace from an individual mouse receiving a formalin injection showing lPBN Y1R neuron activity, licking bouts and smoothed licking behaviour. **e**, Representative trace as shown in **d** along with Gaussian curves. **f**, Correlations between fit and signal for the two fitting methods ($n = 9$ mice; paired two-sided *t*-test on Fisher's *z* values, $P = 0.0055$). **g**, A Cre-off approach to record calcium dynamics of non-Y1R neurons with image showing GCaMP6s expression in non-Y1R neurons. Scale bar, 200 µm. **h**, Average Δ*F*/*F* of GCaMP6s signal from non-Y1R neurons after formalin injection. **i**, Mean Δ*F*/*F* of lPBN non-Y1R neurons ($n = 6$ mice; one-way ANOVA, not significant). **j**, Representative trace from an individual mouse receiving formalin injection showing non-Y1R neuron activity, licking bouts and smoothed licking behaviour. **k**, Representative trace as shown in **j** along with Gaussian curves. **l**, Correlations between fit and signal for Y1R neurons and non-Y1R neurons ($n = 9$ Y1R, $n = 6$ non-Y1R mice; unpaired two-sided *t*-test on Fisher's *z* values, $P = 0.0006$). **m**, A head-mounted miniature microscope was used to record activity of individual lPBN Y1R neurons. Inset, GCaMP6s expression in Y1R neurons. Scale bar, 200 µm. Units were identified using constrained nonnegative matrix factorization (CNMF)[45] after video preprocessing and motion correction. **n**, Heat plot showing calcium fluorescence intensity in response to a formalin injection. Neuron classifications across all recorded neurons from five mice are shown. **o**,**p**, Average fluorescence (**o**) and examples traces (**p**) of neurons classified as lick-activated or pain-activated from the data shown in **n**. Data are mean ± s.e.m. Grey dots and lines represent individual mice.

of NPY to suppress persistent inflammatory and chronic neuropathic pain. We found that unilateral NPY infusion into the lPBN was sufficient to alleviate hypersensitivity to mechanical stimulation following persistent inflammatory injury without affecting inflammation (Extended Data Fig. 6a–c). Similarly, NPY infusion into the lPBN attenuated cold and mechanical allodynia following SNI (Extended Data Fig. 6d,e).

Because hunger-evoked NPY release suppresses persistent inflammatory pain[27], we reasoned that there may be multiple endogenous analgesic circuits that release NPY. In vivo monitoring of NPY in the lPBN with a genetically encoded fluorescent sensor revealed that NPY levels were increased in the lPBN during hunger and thirst, suggesting that these need states may affect persistent pain by acting on NPY receptors in the lPBN (Supplementary Fig. 8). We found that 24 h food deprivation strongly suppressed wound licking during sustained formalin-induced pain (Fig. 3a,b and Extended Data Fig. 7a), mechanical allodynia due to CFA-induced persistent inflammation (Fig. 3c and Extended Data Fig. 7c), and SNI-induced mechanical and cold allodynia (Fig. 3d and Extended Data Fig. 7d). Water deprivation or inducing hypovolemic

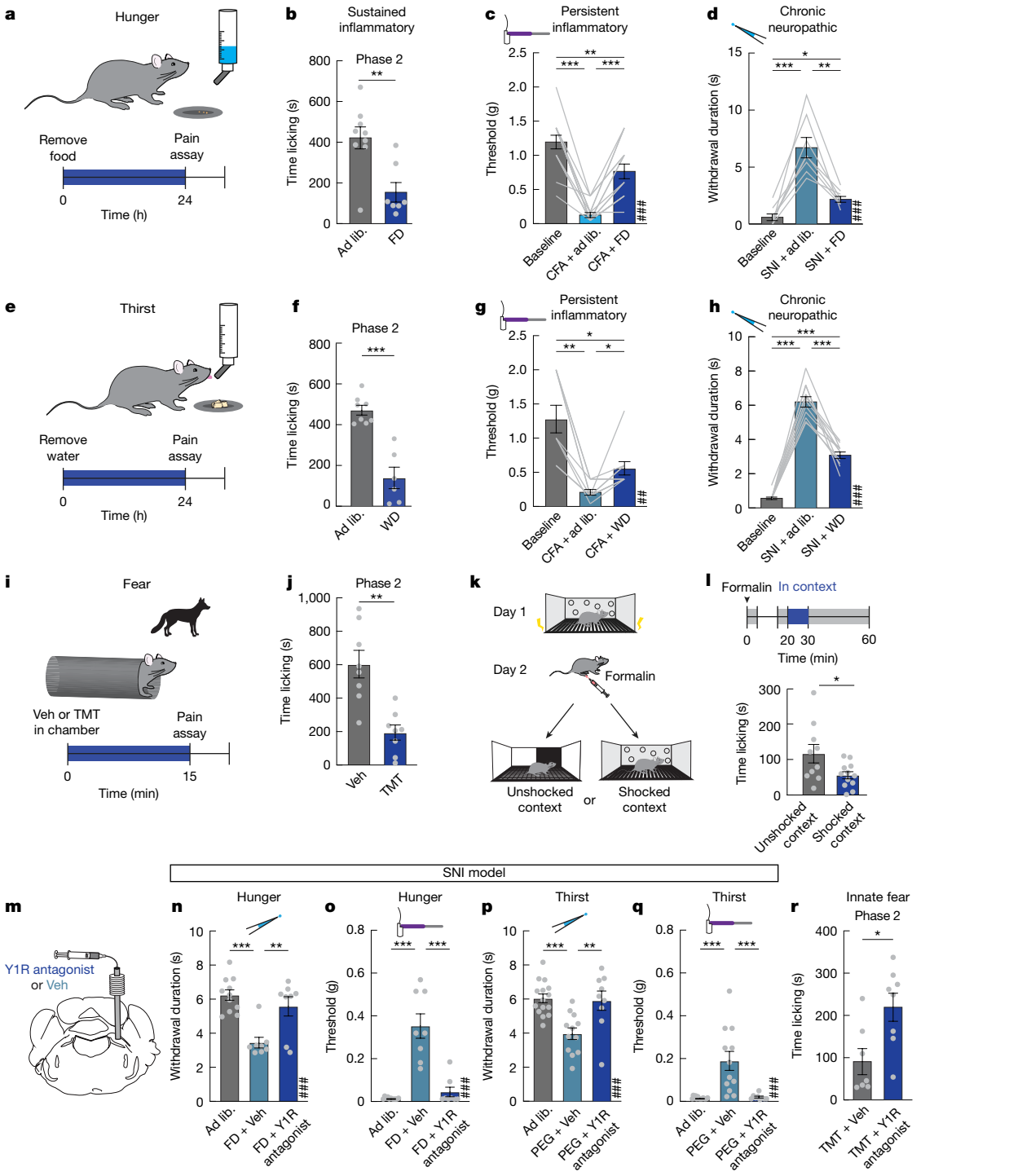

Fig. 3 | Prolonged pain-related responses are suppressed by lPBN NPY–Y1R signalling during competing needs. a, Experimental timeline. **b**, Time licking paw during phase 2 in ad libitum (ad lib.)-fed ($n = 7$) and food-deprived (FD) ($n = 9$) mice (unpaired two-sided t-test, $P = 0.0025$). **c**, Withdrawal threshold to mechanical stimuli in the CFA model ($n = 15$ mice; one-way ANOVA, $P < 0.001$). **d**, Withdrawal duration after acetone application in the SNI model ($n = 8$ mice; one-way ANOVA, $P < 0.001$). **e**, Experimental timeline. **f**, Time licking paw during phase 2 in mice with ad libitum water access ($n = 8$) and water-deprived (WD) ($n = 6$) mice (unpaired two-sided t-test, $P = 0.0007$). **g**, Withdrawal threshold to mechanical stimuli in the CFA model ($n = 10$ mice, one-way ANOVA, $P = 0.0012$). **h**, Withdrawal duration after acetone application in the SNI model ($n = 11$ mice; one-way ANOVA, $P < 0.001$). **i**, Experimental timeline. **j**, Time licking paw during phase 2 in mice with vehicle or TMT in the chamber ($n = 8$ mice per group; unpaired two-sided t-test, $P = 0.0012$). **k**, Experimental timeline. **l**, Time licking after formalin injection while animals were in either in the unshocked ($n = 10$) or the shocked context ($n = 12$) (unpaired two-sided t-test, $P = 0.0495$. **m**, A Y1R antagonist or vehicle was infused into the lPBN. **n**,**o**, Withdrawal threshold to cold (**n**; acetone) or mechanical (**o**) stimuli in ad libitum-fed ($n = 11$) or food-deprived ($n = 8$) mice with a vehicle or Y1R antagonist infusion. All mice had undergone SNI surgery 2 weeks prior (one-way ANOVA, $P < 0.001$). **p**,**q**, Withdrawal threshold to cold (**p**, acetone) or mechanical (**q**) stimuli in mice with ad libitum water ($n = 15$) and PEG-treated mice with a vehicle ($n = 12$) or Y1R antagonist ($n = 9$) infusion (one-way ANOVA, $P < 0.001$). All mice had undergone SNI surgery two weeks prior. **r**, Time licking paw during phase 2 in mice exposed to TMT ($n = 7$ vehicle, $n = 8$ Y1R antagonist mice; unpaired two-sided t-test, $P = 0.0137$). Data are mean ± s.e.m. Grey dots and lines represent individual mice.

thirst with a peripheral injection of polyethylene glycol (PEG) also reduced pain responses in all three pain models (Fig. 3e–h and Extended Data Fig. 7e–q). Unlike the responses during longer-term inflammatory or neuropathic sensitization, hunger and thirst did not affect acute responses to formalin-induced pain (Extended Data Fig. 7b,f,l).

We found that external threats similarly suppressed sustained responses to injury. Introduction of a predator odour (TMT) or an environment previously associated with an aversive shock stimulus both attenuated responses to formalin (Fig. 3i–l and Extended Data Fig. 7s,t). Although these stimuli elicit behaviours such as freezing and avoidance that could interfere with coping behaviours such as paw licking and withdrawal, we found that withdrawal, licking and jumping responses to noxious heat were unaffected by predator odour (Extended Data Fig. 7u–x). Moreover, conditioned fear did not affect responses to formalin when mice were placed in the chamber during the acute phase (Extended Data Fig. 7r), demonstrating that animals are still able to attend to noxious stimuli and perform basic coping behaviours (Supplementary Information). Together, these results point to the existence of NPYergic pathways that are activated by acute threats and selectively suppress long term pain. Monosynaptic rabies tracing experiments revealed several populations of NPY neurons that project to the lPBN (Extended Data Fig. 8a,b and Supplementary Fig. 9). Similar to Y1R neurons, the axons of these populations are distributed throughout the lPBN (Extended Data Fig. 8c–i). Notably, one NPY population located in the subparafascicular nucleus of the thalamus (Supplementary Fig. 9) was activated by TMT, whereas arcuate NPY neurons responded only to hunger (Extended Data Fig. 8j–q). We found that direct connectivity between NPYergic inputs and lPBN Y1R neurons is not essential for the modulation of Y1R neurons, as we find no evidence of synaptic connectivity between arcuate NPY neurons and lPBN Y1R neurons (Extended Data Fig. 8r–w). Thus, incoming NPYergic axons are capable of influencing pain behaviour by acting on Y1R-expressing neurons extrasynaptically through bulk release of NPY throughout the lPBN[23] (Extended Data Fig. 8x).

We next sought to identify the cellular site of NPY-NPY1R interaction that suppresses pain during competing needs. Blocking the Y1 receptor with a local antagonist infusion occluded the analgesic effects of hunger, thirst and innate fear[27] (Fig. 3m–r and Supplementary Fig. 10a,b). The effect of blocking NPY signalling was specific to sustained pain behaviour, as we did not observe changes in acute nociception or mobility (Supplementary Fig. 10c,d). Further, the Y1R antagonist did not change behavioural responses in the absence of competing needs (Supplementary Fig. 10e–g), nor did it influence fear responses in the absence of injury (Supplementary Fig. 10h,i). Because Y1 receptors affect neurotransmission both pre- and post-synaptically[29–31] we explored the function of the Y1 receptor on both spinoparabrachial and lPBN neurons (Extended Data Fig. 9a,b). Genetic deletion of Y1R in the dorsal horn[32] did not affect the ability of hunger to suppress pain (Extended Data Fig. 9c). Conversely, reducing Y1R expression in the lPBN did block the analgesic effect of hunger (Extended Data Fig. 9d). These results suggest that the endogenous release of NPY in the lPBN mediates analgesia during acute survival threats by acting on the postsynaptic Y1R expressed on lPBN neurons. Thus, lPBN Y1R neurons could be a critical hub for the convergence of hunger, thirst and fear that gate persistent pain to promote survival.

Gating of nociceptive input by survival threats

We have established that Y1R neurons in the lPBN are activated during sustained responses to noxious stimuli, and that hunger, thirst and fear suppress these pain-related behavioural responses via NPY–Y1R signalling on neurons in the lPBN. Because our indices of pain in mice are limited to observed coping and reflexive behaviours, we next used a mathematical model to infer an internal pain state based on these behaviours. We modelled behaviour as a negative feedback process, starting from the assumptions that animals aim to reduce pain with minimal action or 'effort', and that licking is a coping behaviour that reduces pain at the cost of some effort. Thus, our model system incorporates two state variables—perceived pain and exerted effort—and two available actions of doing nothing or licking, where the latter reduces pain at the cost of effort (Fig. 4a and Extended Data Fig. 10a,b). We next used Q-learning, a type of reinforcement learning, to learn a control policy for production of licking given the pain and effort state variables. We found that the two-dimensional state space of pain and effort was sufficient to match the observed behavioural response to formalin injection in baseline conditions (Fig. 4b–d).

We next used this model to evaluate potential ways in which a competing need signal (conveyed via NPY) might affect both behaviour and the underlying pain state. We performed three modulations: (1) gating the integration of ascending nociceptive input to reduce perceived pain; (2) increasing the effort 'cost' of coping behaviour to reduce behavioural response to pain; or (3) acting as a third 'state' axis of a control policy to enable higher-dimensional mappings from state to behaviour (Supplementary Information). We retrained a set of models using a 'competing need state' condition, in which for each model we modulated one of the three potential sites of action (Fig. 4a and Extended Data Fig. 10c,d). The model incorporating gating of ascending pain integration predicted a substantial decrease in licking behaviour during the inflammatory phase, closely mirroring the behaviour observed in mice. This model also predicted a decrease in underlying pain state (Fig. 4e–i and Extended Data Fig. 10g–i). By contrast, manipulations that modulated the effort cost per lick or the behavioural policy itself did not significantly alter behavioural responses and predicted an increase, rather than a decrease, in the underlying pain state of the model in the presence of a competing need signal (Fig. 4j–m and Extended Data Fig. 10e,f,j–o). This finding suggests that NPY modulates behaviour by gating the integration of ascending nociceptive input.

We noted that the model's pain and effort states in the baseline condition resembled the slow and fast dynamics, respectively, of Y1R neural activity after formalin injection (Fig. 2b,e,n,o). This suggests that activity in tonically activated Y1R neurons may reflect pain state. To determine how the modelled pain state compared to Y1R neuron activity during competing needs, we measured lPBN Y1R population calcium dynamics in response to noxious stimuli during hunger, thirst and innate fear. Hunger (food deprivation), thirst (PEG) and fear (TMT) each eliminated the Y1R neural response during the inflammatory phase of the formalin assay (Fig. 5a–f), mirroring the observed suppression of behavioural responses. According to our model, this finding further suggests that NPY acts as a competing need signal that gates ascending nociceptive input. The reduction in Y1R neural activity was recapitulated by chemogenetic activation of arcuate NPY neurons that project to the PBN (Fig. 5g–k), demonstrating that activity of a single endogenous analgesic NPYergic projection is capable of suppressing Y1R neural activity during persistent pain. We also found that the potentiation of Y1R responses to pinching the paw during persistent inflammation was reversed by food deprivation (Fig. 5l–o), indicating that Y1R neural responses to other forms of injury that cause prolonged pain are also modulated by competing need states. By contrast, neither food deprivation nor NPY neuron stimulation affected Y1R neuron responses to noxious heat (Fig. 5p–r and Supplementary Fig. 11), again mirroring behavioural findings and demonstrating that need states do not change the dynamics of these neurons immediately following acute injury. Together, our modelling and neural recording experiments suggest that the slow component of Y1R neuron activity reflects an ongoing pain state that is independent of coping behaviour and is modified by NPY signalling during competing needs.

Discussion

Deconstructing the various aspects of pain has been a challenge for centuries[6,9,33]. The idea that pain is a global brain and body state rather

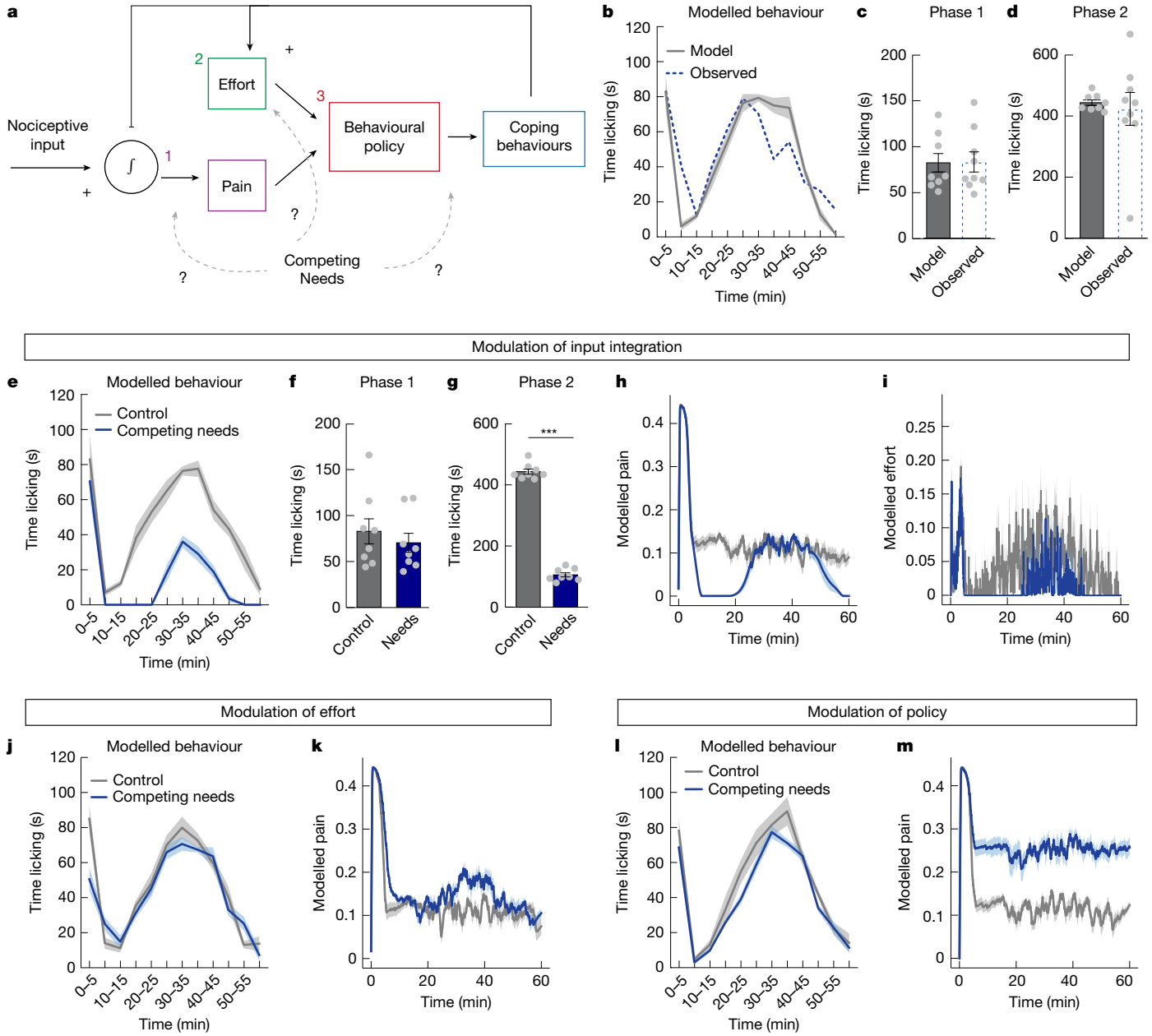

Fig. 4 | IPBN modulation by competing needs is consistent with a gating of nociceptive input. a, Schematic of the model control system for regulating behaviour during pain. Nociceptive input is integrated into an internal 'pain' state, and past actions (licks) are integrated over recent history by an internal 'effort' state. The model's learned policy maps pain and effort states to a generated behaviour (lick or don't lick), which in turn modifies the value of the two states. We study the effect of competing needs by manipulating three different parts of the model (input integration, effort and policy (dotted arrows)). **b**, Time spent licking paw in 5-min bins of 8 trained models compared with observed mouse behaviour. **c**,**d**, Time spent licking paw in phase 1 (**c**) and phase 2 (**d**) ($n = 8$ model runs, $n = 9$ observed mice). **e**, Simulated paw-licking behaviour of eight trained models, comparing control with a competing need that reduces nociceptive integration. **f**,**g**, Simulated time licking paw in phase 1 (**f**) and phase 2 (**g**) in the models ($n = 8$ model runs per condition; unpaired two-sided t-test, not significant (**f**), $P < 0.001$ (**g**)). **h**,**i**, Average dynamics of the pain (**h**) and effort (**i**) states of eight trained models, comparing control with a competing need that reduces nociceptive integration. **j**,**k**, Simulated paw-licking behaviour (**j**) and average pain state dynamics (**k**) of eight trained models, comparing control with a competing need that increases the effort cost of licking. **l**,**m**, Simulated paw licking behaviour (**l**) and average pain state dynamics (**m**) of eight trained models, comparing control with a competing need that extends the dimension of the policy. Data are mean ± s.e.m. Grey dots represent individual mice or individual model runs.

than a transient sensory experience has become widely accepted[34]. Identifying, describing and quantifying this state, especially in pre-clinical models, is an important step in developing treatments for pain. Assessing pain state, however, requires going beyond traditional behavioural measures, as pain states persist when animals are not actively engaged in coping behaviours[35]. For example, unbiased computational assessments of posture or facial expressions have recently been used to infer emotional states including the negative affect associated with pain[36]. Here we find evidence for two additional indices of pain state—neurophysiological signatures of longer lasting pain states and behavioural modelling based on control theory. These methods can also ultimately be used to test how pain states are affected by physiological, environmental or therapeutic interventions.

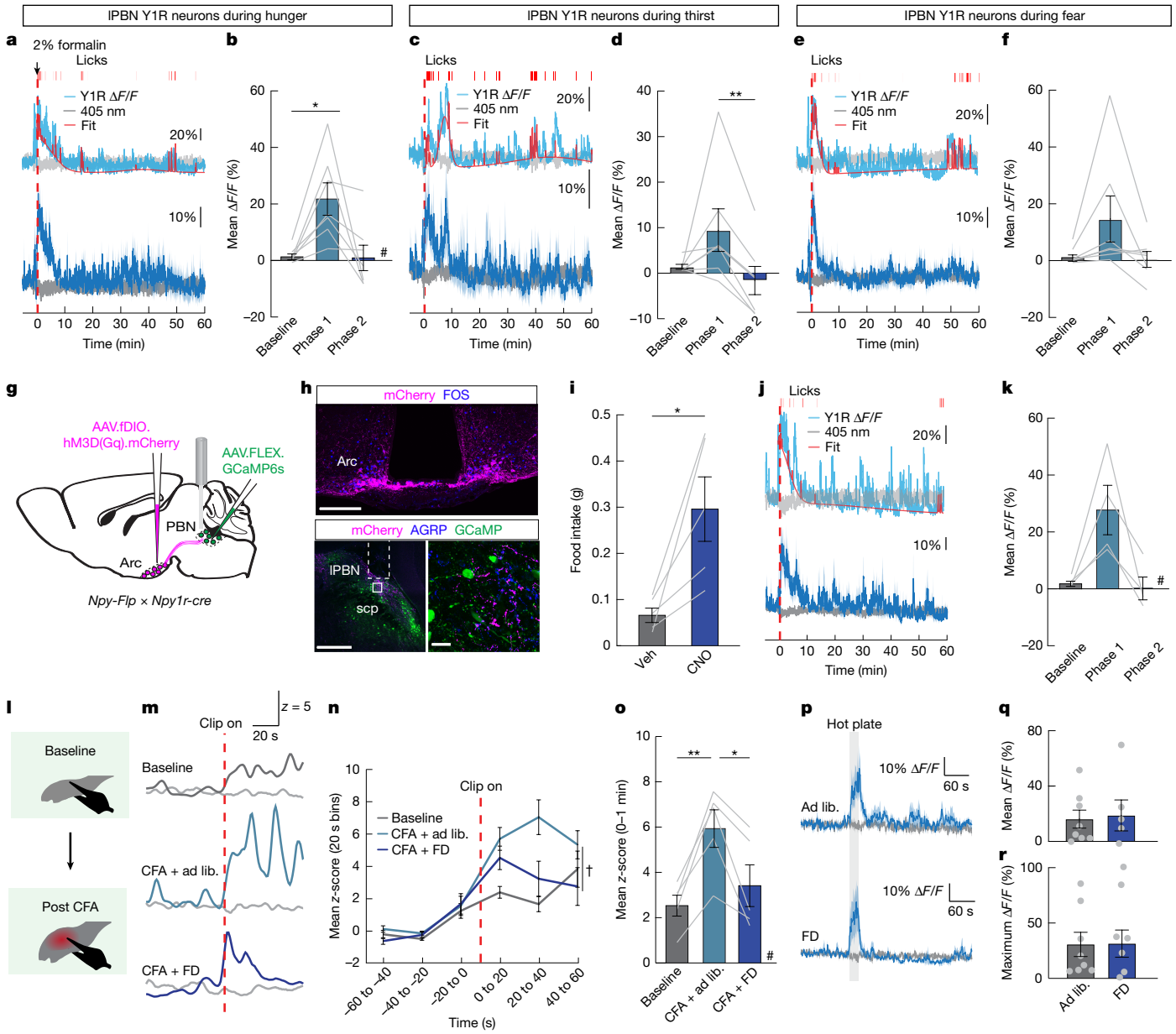

Fig. 5 | Competing survival threats suppress lPBN Y1R neuron responses during persistent pain. a, Representative (top) and average (bottom) Δ*F*/*F* of GCaMP6s signal of Y1R neurons, paw licking bouts and smoothed licking behaviour after formalin in food-deprived mice. **b**, Mean Δ*F*/*F* of lPBN Y1R neurons in food-deprived mice ($n = 7$ mice; one-way ANOVA, $P = 0.0156$). **c**, Representative (top) and average (bottom) Δ*F*/*F* of GCaMP6s signal of Y1R neurons after formalin in PEG-treated, thirsty mice. **d**, Mean Δ*F*/*F* of lPBN Y1R neurons in PEG-treated thirsty mice ($n = 7$ mice; one-way ANOVA, $P = 0.0523$). **e**, Representative (top) and average (bottom) Δ*F*/*F* of GCaMP6s signal of Y1R neurons after formalin in mice exposed to TMT. **f**, Mean Δ*F*/*F* of lPBN Y1R neurons in TMT-exposed mice ($n = 7$ mice; one-way ANOVA, not significant). **g**, Strategy to record Y1R neurons during evoked activation of arcuate NPY neurons. **h**, Top and bottom left, hM3D(Gq)-mCherry expression in the arcuate nucleus (Arc) with FOS expression after a CNO injection along with GCaMP expression in Y1R neurons. Scale bars, 200 µm. Bottom right, magnified image of the area inside the white dashed line. Scale bar, 20 µm. scp, superior cerebellar peduncle. **i**, Food consumption ($n = 5$ mice; paired two-sided *t*-test, $P = 0.0269$). **j**, Representative (top) and average (bottom) Δ*F*/*F* of GCaMP6s signal in Y1R neurons in ad libitum-fed mice with arcuate NPY neurons activated. **k**, Mean Δ*F*/*F* of lPBN Y1R neurons after NPY neuron stimulation ($n = 4$ mice; one-way ANOVA, $P = 0.0348$). **l**, Experimental timeline. **m**, Trace of Y1R neuron GCaMP6s signal in responses to pinch. **n**. Average *z*-score (20-s bins) during the pinch test shown in **m** ($n = 5$ mice; two-way ANOVA, group × time interaction $P = 0.0221$). **o**, Mean *z*-score after the pinch is applied to the paw in the three groups shown in **m** ($n = 5$ mice; one-way ANOVA, $P = 0.0158$). **p**, Average Δ*F*/*F* of GCaMP6s signal from Y1R neurons while ad libitum-fed or food-deprived mice were placed on a 52 °C hot plate for 20 s (grey shaded region). **q**, Mean Δ*F*/*F* of GCaMP6s signals shown in **p** during the hot plate period ($n = 8$ ad libitum, $n = 6$ FD; unpaired two-sided *t*-test, not significant). **r**, Maximum Δ*F*/*F* of GCaMP6s signals shown in **p** during hot plate period ($n = 8$ ad libitum, $n = 6$ FD; unpaired two-sided *t*-test, not significant). Data are mean ± s.e.m. Grey dots and lines represent individual mice.

Using neural activity recordings and modelling, we show that persistent pain states lead to sustained activity selectively in Y1R neurons of the lPBN. Prolonged pain in the absence of an external noxious stimulus is likely to reflect changes in peripheral systems and central neural networks that relay information to the brain[12,37–40]. As the PBN is a key brain site to which spinal nociceptive pathways project, the Y1R neurons are positioned to serve as a sensor for persistent pain. We find the Y1R neurons are both spatially[41] and molecularly[25,26] distributed across previously identified PBN regions and neuron populations. The Y1 receptor is expressed in roughly 20% of the functional and molecular subclasses

of neurons that have previously been identified to modulate specific pain behaviours in response to noxious stimuli or different types of injury[13,14,22,42,43] (Supplementary Table 4). Thus, Y1R neurons in the PBN are positioned to sample various inputs and influence outputs of many PBN neuron types. This ensemble appears to be less important for signalling the acute responses to specific injuries or transient noxious stimuli but rather serves as a sentinel for ongoing affective changes and coping behaviours that occur following injury.

The distribution of Y1R neurons throughout the PBN suggests that these neurons are uniquely positioned to monitor the state of the animal, similar to the privileged role of Y1R-expressing neurons in the hypothalamus[44]. Our findings suggest that a variety of acute physiological and environmental needs can specifically alleviate sustained responses to injury without affecting acute nociception. We identified the Y1R neurons of the PBN as a central hub for the convergence of needs states that allows for the gating of sustained pain through NPY signalling. This suggests that endogenous analgesic circuits have evolved to suppress pain by reducing the integration of noxious sensory input, and this is a common mechanism used by various survival needs to determine pain behaviour. This mechanism is an efficient and tunable system that enables urgent needs to shift brain state away from pain and towards other states that promote survival[23]. Future work could build from these findings to test other endogenous or pharmacological interventions that curb pain state.

Online content

Any methods, additional references, Nature Portfolio reporting summaries, source data, extended data, supplementary information, acknowledgements, peer review information; details of author contributions and competing interests; and statements of data and code availability are available at https://doi.org/10.1038/s41586-025-09602-x.

1. Maier, C. et al. Quantitative sensory testing in the German Research Network on Neuropathic Pain (DFNS): Somatosensory abnormalities in 1236 patients with different neuropathic pain syndromes. *Pain* **150**, 439–450 (2010).
2. Duan, B. et al. Identification of spinal circuits transmitting and gating mechanical pain. *Cell* **159**, 1417–1432 (2014).
3. Wilson, T. D. et al. Dual and opposing functions of the central amygdala in the modulation of pain. *Cell Rep.* **29**, 332–346.e5 (2019).
4. Zhao, R. et al. Neuropathic pain causes pyramidal neuronal hyperactivity in the anterior cingulate cortex. *Front. Cell Neurosci.* **12**, 107 (2018).
5. Mogil, J. S. Animal models of pain: progress and challenges. *Nat. Rev. Neurosci.* **10**, 283–294 (2009).
6. Lindsay, N. M., Chen, C., Gilam, G., Mackey, S. & Scherrer, G. Brain circuits for pain and its treatment. *Sci. Transl. Med.* **13**, eabj7360 (2021).
7. Peirs, C. & Seal, R. P. Neural circuits for pain: recent advances and current views. *Science* **354**, 578–584 (2016).
8. Price, T. J. et al. Transition to chronic pain: opportunities for novel therapeutics. *Nat. Rev. Neurosci.* **19**, 383–384 (2018).
9. Basbaum, A. I., Bautista, D. M., Scherrer, G. & Julius, D. Cellular and molecular mechanisms of pain. *Cell* **139**, 267–284 (2009).
10. Corder, G. et al. An amygdalar neural ensemble that encodes the unpleasantness of pain. *Science* **363**, 276–281 (2019).
11. Dubin, A. E. & Patapoutian, A. Nociceptors: the sensors of the pain pathway. *J. Clin. Invest.* **120**, 3760–3772 (2010).
12. Choi, S. et al. Parallel ascending spinal pathways for affective touch and pain. *Nature* **587**, 258–263 (2020).
13. Deng, J. et al. The parabrachial nucleus directly channels spinal nociceptive signals to the intralaminar thalamic nuclei, but not the amygdala. *Neuron* **107**, 909–923.e6 (2020).
14. Barik, A. et al. A spinoparabrachial circuit defined by Tacr1 expression drives pain. *eLife* **10**, e61135 (2021).
15. Yang, H. et al. Pain modulates dopamine neurons via a spinal–parabrachial–mesencephalic circuit. *Nat. Neurosci.* **24**, 1402–1413 (2021).
16. Melzack, R. & Wall, P. D. Pain mechanisms: a new theory. *Science* **150**, 971–978 (1965).
17. WALL, P. D. The gate control theory of pain mechanisms: a re-examination and re-statement. *Brain* **101**, 1–18 (1978).
18. Tracey, I., Woolf, C. J. & Andrews, N. A. Composite pain biomarker signatures for objective assessment and effective treatment. *Neuron* **101**, 783–800 (2019).
19. Woo, C.-W., Chang, L. J., Lindquist, M. A. & Wager, T. D. Building better biomarkers: brain models in translational neuroimaging. *Nat. Neurosci.* **20**, 365–377 (2017).
20. Sun, L. et al. Parabrachial nucleus circuit governs neuropathic pain-like behavior. *Nat. Commun.* **11**, 5974 (2020).
21. Condon, L. F. et al. Parabrachial Calca neurons drive nociplasticity. *Cell Rep.* **43**, 114057 (2024).
22. Chiang, M. C. et al. Divergent neural pathways emanating from the lateral parabrachial nucleus mediate distinct components of the pain response. *Neuron* **106**, 927–939.e5 (2020).
23. van den Pol, A. N. Neuropeptide transmission in brain circuits. *Neuron* **76**, 98–115 (2012).
24. Karthik, S. et al. Molecular ontology of the parabrachial nucleus. *J. Comp. Neurol.* **530**, 1658–1699 (2022).
25. Pauli, J. L. et al. Molecular and anatomical characterization of parabrachial neurons and their axonal projections. *eLife* **11**, e81868 (2022).
26. Nardone, S. et al. A spatially-resolved transcriptional atlas of the murine dorsal pons at single-cell resolution. *Nat. Commun.* **15**, 1966 (2024).
27. Alhadeff, A. L. et al. A neural circuit for the suppression of pain by a competing need state. *Cell* **173**, 140–152.e15 (2018).
28. Campos, C. A., Bowen, A. J., Roman, C. W. & Palmiter, R. D. Encoding of danger by parabrachial CGRP neurons. *Nature* **555**, 617–622 (2018).
29. Chen, G. & van den Pol, A. N. Multiple NPY receptors coexist in pre- and postsynaptic sites: inhibition of GABA release in isolated self-innervating SCN neurons. *J. Neurosci.* **16**, 7711–7724 (1996).
30. Browning, K. N. & Travagli, R. A. Neuropeptide Y and peptide YY inhibit excitatory synaptic transmission in the rat dorsal motor nucleus of the vagus. *J. Physiol.* **549**, 775–785 (2003).
31. Zhang, X., Tong, Y., Bao, L. & Hökfelt, T. The neuropeptide Y Y1 receptor is a somatic receptor on dorsal root ganglion neurons and a postsynaptic receptor on somatostatin dorsal horn neurons. *Eur. J. Neurosci.* **11**, 2211–2225 (1999).
32. Nelson, T. S. et al. Spinal neuropeptide Y Y1 receptor-expressing neurons are a pharmacotherapeutic target for the alleviation of neuropathic pain. *Proc. Natl Acad. Sci. USA* **119**, e2204515119 (2022).
33. Rey, R. *The History of Pain* (Harvard Univ. Press, 1998).
34. Craig, A. D. A new view of pain as a homeostatic emotion. *Trends Neurosci.* **26**, 303–307 (2003).
35. Cobos, E. J. & Portillo-Salido, E. "Bedside-to-bench" behavioral outcomes in animal models of pain: beyond the evaluation of reflexes. *Curr. Neuropharmacol.* **11**, 560–591 (2013).
36. Jhumka, Z. A. & Abdus-Saboor, I. J. Next generation behavioral sequencing for advancing pain quantification. *Curr. Opin. Neurobiol.* **76**, 102598 (2022).
37. Peirs, C. et al. Mechanical allodynia circuitry in the dorsal horn is defined by the nature of the injury. *Neuron* **109**, 73–90.e7 (2021).
38. Huang, T. et al. Identification of pathways required for sustained pain-associated coping behaviors. *Nature* **565**, 86–90 (2019).
39. Todd, A. J. Identifying functional populations among the interneurons in laminae I–III of the spinal dorsal horn. *Mol. Pain* **13**, 1744806917693003 (2017).
40. Yarmolinsky, D. A. et al. Differential modification of ascending spinal outputs in acute and chronic pain states. *Neuron* **113**, 1223–1239.e5 (2025).
41. Fulwiler, C. E. & Saper, C. B. Subnuclear organization of the efferent connections of the parabrachial nucleus in the rat. *Brain Res. Rev.* **7**, 229–259 (1984).
42. Barik, A., Thompson, J. H., Seltzer, M., Ghitani, N. & Chesler, A. T. A brainstem–spinal circuit controlling nocifensive behavior. *Neuron* **100**, 1491–1503.e3 (2018).
43. Liu, S. et al. Divergent brainstem opioidergic pathways that coordinate breathing with pain and emotions. *Neuron* **110**, 857–873.e9 (2022).
44. Xu, S. et al. Behavioral state coding by molecularly defined paraventricular hypothalamic cell type ensembles. *Science* **370**, eabb2494 (2020).
45. Zhou, P. et al. Efficient and accurate extraction of in vivo calcium signals from microendoscopic video data. *eLife* **7**, e28728 (2018).

Methods

Experimental model and subject details

Mice were group-housed on a 12 h light:12 h dark cycle with ad libitum access to food (Purina Rodent Chow, 5001) and water unless otherwise noted. Temperature (21.5–22.3 °C) and humidity (50 ± 15%) were controlled. Group-housed adult male and female mice (at least eight weeks old) were used for experiments. *Npy1r-cre* (Jackson Laboratory 030544, *B6.Cg-Npy1r*$^{tm1.1(cre/GFP)Rpa}$/J (ref. 46), *Npy-Flp* (Jackson Laboratory 030211, *B6.Cg-Npy*$^{tm1.1(flpo)Hze}$/J)[47], *Pdyn-IRES-cre* (Jackson Laboratory 027958, B6;129S-*Pdyn*$^{tm1.1(cre)Mjkr}$/LowlJ)[48], *Penk-IRES2-cre* (Jackson Laboratory 025112, B6;129S-*Penk*$^{tm2(cre)Hze}$/J), *Vglut2-IRES-cre* (Jackson Laboratory 016963, *Slc17a6*$^{tm2(cre)Lowl}$/J)[49], *Y1-lox/lox* (*Npy1r*$^{lox/lox}$; ref. 50), *Lbx1-cre* (*Lbx1*$^{tm3.1(cre)Cbm}$)[51], *Npy-IRES-cre* (Jackson Laboratory 027851, B6.Cg-*Npy*$^{tm1(cre)Zman}$/J)[52], *Agrp-IRES-cre* (Jackson Laboratory 012899, *Agrp*$^{tm1(cre)Lowl}$/J)[53], *NPY-hrGFP* (Jackson Laboratory 006417, B6.FVB-Tg(Npy-hrGFP)1Lowl/J) and C57BL/6J mice were used for experiments. Genotyping of the *Y1-lox/lox* mice was performed using primers and conditions provided by Jackson Laboratory. All other strains were genotyped by Transnetyx. Sample sizes were chosen based on standards in the neuroscience field and our prior data. All mice were habituated to handling and experimental conditions prior to experiments. For within-subject behavioural analyses, all mice received all experimental conditions. Conditions were counter balanced unless otherwise noted, and order was randomly assigned. For between-subject analyses, mice were randomly assigned to experimental condition. In experiments where data were analysed post hoc (formalin, hot plate, fibre photometry and miniscope) blinding was performed during data analysis. In experiments where behaviour was analysed by investigators collecting the data (von Frey test and acetone test), blinding was performed prior to data collection. We performed experiments in both male and female subjects and did not observe any significant sex differences. All procedures were approved by the University of Pennsylvania, University of Florida and University of Pittsburgh Institutional Animal Care and Use Committees.

Spatial transcriptomics

Tissue collection and sectioning. Transcardial perfusion with ice-cold saline was performed 1 h after formalin injection (see below). Following perfusion to remove circulating blood, brains were quickly dissected and placed on an aluminium foil boat in liquid nitrogen for rapid freezing. Once frozen, the brains were transferred to a 25 ml conical tube and submerged in liquid nitrogen for an additional 10 min. Fully frozen brains were stored at −80 °C overnight prior to sectioning. Frozen brains were transferred to a pre-cooled (−20 °C) cryostat and allowed to equilibrate to the chamber temperature. Brains were then mounted and coronal sections (10 µm thickness) were collected at −5.20 mm from bregma and mounted onto VWR Superfrost Plus Micro Slides, ensuring placement within the 15 mm × 20 mm scan area required for the CosMx spatial molecular imager. Slides were kept within the cryostat chamber at −20 °C throughout the sectioning process and stored at −80 °C overnight. Tissue was collected from three mice, with two slides containing six sections each (two from each mouse).

Slide preparation and in situ hybridization. All procedures were performed according to manufacturer specifications.

NBF fixation and baking. Slides were removed from −80 °C storage and immediately placed into ice-cold 10% neutral buffered formalin (NBF) for a 2 h fixation. Following fixation, slides were washed three times with 1× phosphate-buffered saline (PBS) to remove residual fixative. Slides were then positioned vertically and baked at 60 °C for 30 min to enhance tissue adhesion.

Tissue dehydration and target retrieval. Slides were incubated in 4% SDS to remove residual lipids and proteins, followed by serial dehydration using increasing concentrations of ethanol. For target retrieval, slides were immersed in a pre-warmed retrieval solution and incubated at 100 °C for 20 min. After retrieval, slides were washed in PBS, dehydrated with 100% ethanol and air-dried at room temperature for 30 min.

Tissue permeabilization. Brucker-supplied incubation frames were applied to the slides, outlining the scan area containing the tissue. The digestion buffer was prepared by diluting proteinase K and protease A in protease A buffer as the diluent. Four-hundred microlitres of the digestion buffer was applied to each slide, ensuring complete coverage of the tissue within the incubation frame. Slides were incubated at room temperature for 30 min to facilitate tissue permeabilization. Following incubation, slides were washed thoroughly with 1× PBS to remove residual enzymes.

Fiducial preparation, application and post-fixation. Brucker-supplied fiducial stock solution underwent a five-step sonication and vortex process to ensure uniform dispersion. The stock solution (0.1%) was diluted to 0.00015% using 2× SCC-T solution through a two-step serial dilution to maintain dilution accuracy. For fiducial application, 250 µl of the diluted fiducial solution was applied per slide, thoroughly mixing by vortex before each application to prevent fiducial clumping. Slides were incubated at room temperature for 5 min, followed by a PBS wash to remove excess fiducials. Immediately after washing, slides were transferred into 10% NBF for 1 min for post-fixation. Fixation was then halted using the NBF stop buffer (Tris-glycine buffer), and slides were subsequently stored in 1× PBS.

NHS-acetate preparation and application. Pre-prepared NHS-acetate powder aliquots were carefully mixed with Bruker-supplied NHS-acetate buffers by pipetting up and down slowly to prevent bubble formation, yielding a 100 mM solution. Two hundred and fifty microlitres of the prepared buffer was applied to each slide within the incubation frame. Slides were incubated at room temperature for 15 min in a light-protected staining tray to prevent photodegradation. Following incubation, slides were thoroughly washed with 2× SSC solution to remove excess buffer.

Overnight in situ hybridization. The 1,000-plex mouse neuroscience RNA probe mix, custom probe mix, and ribosomal RNA (rRNA) segmentation markers were aliquoted into PCR tubes and denatured at 95 °C for 2 min in a preheated thermal cycler. Immediately after denaturation, the aliquots were crash-cooled on ice for at least 1 min to prevent reannealing. The hybridization mix was prepared by combining: 1,000-plex mouse neuroscience RNA probe mix, custom probe mix, rRNA segmentation markers, RNA inhibitor and Bruker-supplied buffer R. One-hundred and fifty microlitres of the hybridization mix was applied to each slide within the incubation frame, and an incubation frame cover was placed over the frame to prevent evaporation. Slides were then transferred to a hybridization tray lined with wipes soaked in 2× SSC, creating a humid chamber to maintain optimal hybridization conditions. The tray was placed in a hybridization oven at 37 °C for 16–18 h overnight to allow for probe–target binding.

Stringent wash. Two batches of stringent wash solution were prepared by mixing 100% formamide and 4× SSC solution in a 1:1 ratio within a 50 ml conical tube. The solution was incubated in a 37 °C water bath for at least 30 min to equilibrate to the desired temperature. After hybridization, slides were removed from the hybridization oven, and incubation frame covers were carefully removed. To eliminate residual unbound probes, each slide was briefly dipped in 2× SSC at room temperature. Slides were transferred into the preheated stringent wash solution and incubated twice for 25 min at 37 °C to maintain optimal stringency conditions. Following the stringent washes, slides were washed twice in 2× SSC to remove any remaining formamide.

Nuclear and cell segmentation staining. The nuclear stain (DAPI) buffer was prepared by diluting nuclear stain stock in the Bruker-supplied blocking buffer at a 1:40 ratio. Two-hundred microlitres of the prepared stain was applied to each slide and incubated for 15 min at room temperature, protected from light to prevent photobleaching. Following nuclear staining, slides were washed with 1× PBS to remove excess stain.

The segmentation mix was prepared by diluting GFAP and histone markers in the Bruker-supplied blocking buffer. Staining was performed by applying the segmentation mix to each slide and incubating for 1 h in a humidity chamber, protected from light.

Flow cell assembly. Incubation covers were carefully removed from the slides, and flow cells were placed over the slides to maximize clearance of the scan area. The slide–flow cell system was then positioned into the Bruker-supplied flow cell assembly tool, ensuring precise adhesion of the flow cell to the slide. To prevent sample desiccation, the assembled flow cells were dipped into 2× SSC, allowing the solution to enter through the fluidics ports and maintain hydration.

Instrument set-up and loading and flow cell configuration. A new acquisition was started and the pre-bleaching and cell segmentation profiles specific to mouse neuronal tissue for RNA assays were selected to optimize imaging parameters. Flow cells were then loaded into the instrument, initiating the run. Upon verifying proper reagent flow, segmentation imaging was performed.

CosMx spatial molecular imaging. Following cell segmentation imaging, the CosMx software displayed the segmented image with four fluorescent markers (DAPI, GFAP, rRNA and histone) across four channels. Using the segmentation data for ease of visualization, fields of view (FOVs) were manually selected based on regions of interest for spatial transcriptomics. Each FOV measured 0.51 × 0.51 mm, and approximately 250–300 FOVs were selected per slide, prioritizing areas of the PBN. Once finalized, the instrument initiated reporter cycling, during which the selected FOVs were imaged over a period of approximately 6 days to capture transcriptomic data.

Preprocessing and data integration. Following completion of reporter cycling, data analysis was initiated using the AtoMx Spatial Informatics Platform (SIP).

Cell segmentation validation. The first step involved cell segmentation analysis to verify the accuracy of initial segmentation settings. If segmentation was suboptimal, advanced parameters were adjusted to re-segment cells.

Study creation and quality control. A pipeline of sequential analyses was established using cloud-based processing, beginning with quality control (QC). The QC module flagged: cells with low transcript counts, cells with high negative probe percentages and FOVs with potential artefacts. The QC results indicated no issues with FOVs. One per cent of cells were flagged for low transcript counts.

Normalization and dimensionality reduction. Expression data were normalized from raw counts to account for variability in library size and transcript abundance across cells and FOVs. Seurat's default LogNormalize method was used, where feature counts per cell were divided by the total transcript counts for that cell, and counts were multiplied by a scale factor and then transformed using natural log (log1p). Principal component analysis (PCA) was performed, with 50 principal components computed. PCA results were used to generate a UMAP for visualization, Leiden clustering for identifying distinct cell clusters, and InSituType cell typing, an unsupervised method that detects cell clusters without a reference matrix. Cell types were later assigned based on marker gene expression and cellular characteristics. Visualization outputs included a heatmap of marker genes, aiding in the identification of cell types.

Neighbourhood analysis and spatial composition. To analyse spatial organization, we applied neighbourhood analysis using the cell typing module. This identified distinct cellular niches based on cell type composition and x–y spatial coordinates. Multiple runs were performed with varying distance parameters to uncover emergent spatial patterns at different scales of neighbourhood reach.

Data export and integration. All processed data—including QC metrics, normalized and raw expression values, PCA results, UMAP embeddings, Leiden clustering and neighbourhood analysis outputs—were exported alongside spatial transcript locations, polygon coordinates for cell segmentation boundaries, and FOV positions. Datasets were saved in multiple formats, including Seurat objects (.rds) for integration with R-based pipelines and spreadsheet files (.csv) for Python-based pipelines for further computational analysis.

Data integration, standardization and AnnData construction. Before integrating the datasets, naming conventions and data structures were examined to ensure consistency. Then, a virtual 'stitched' slide was created by adjusting global pixel coordinates and FOV names of slide 2 to ensure ample separation from slide 1. The stitched expression matrix, polygon, metadata, and FOV files were stored as unique variables and used to construct an annotated data (AnnData) object using Scanpy. The raw count matrix (stitched expression matrix.csv file), which contained gene expression values per cell, was converted into a dense 2D NumPy array to ensure compatibility with AnnData. Finally, the integrity of the dataset was verified by checking the dimensions of the AnnData object and previewing the metadata to confirm correct indexing and feature alignment. This structured dataset served as the foundation for all downstream transcriptomic and spatial analyses.

Transcriptomic and spatial analysis of the PBN and neuronal subpopulations. *Region-specific spatial analysis and AnnData refinement.* To accurately isolate the PBN, spatial plots (for example, Leiden clustering and neighbourhood analysis) were exported from Scanpy and overlaid in Adobe Illustrator. Polygon vector outlines were manually drawn to outline each PBN. Since 12 brain sections were imaged, a total of 24 polygons were generated. The polygon layer was then exported as a .png file and dynamically stitched onto a Scanpy-generated spatial plot, ensuring precise alignment with the dataset. The Shapely Python package was used to extract the pixel coordinates of each vectorized polygon. Each polygon was assigned a unique identifier based on the slide number, brain section, and hemisphere. The pixel coordinates defining each polygon were stored as predefined Shapely polygons within a dictionary. The spatial coordinates of all cells were extracted from adata.obsm["spatial"], and the function assign_polygon_labels() iterated through each cell to determine if it fell within any of the predefined polygons using Shapely's.contains() method. A Boolean mask was applied to exclude cells outside of the designated regions, and a new AnnData object was generated, containing only cells within the identified PBN regions. The new adata also contains the PBN unique identifier created for each polygon, stored in the obs attribute.

Quality control and filtering. Quality control steps were performed using Scanpy's preprocessing module to filter out low-quality cells and lowly expressed genes. Cells with fewer than 100 detected transcripts were removed using scanpy.pp.filter_cells(). Additionally, genes expressed in fewer than 400 cells were removed using scanpy.pp.filter_genes().

Normalization and dimensionality reduction. To preserve raw transcriptomic data, the primary expression matrix (X) was copied into a new layer (adata.layers["counts"]) before performing normalization. Global scaling was applied using scanpy.pp.normalize_total(), which normalizes transcript counts to 10,000 per cell to correct for variations in sequencing depth. A natural log transformation (scanpy.pp.log1p()) was then applied to the normalized counts to reduce the influence of outliers and approximate a normal distribution for improved statistical analyses. PCA was performed using scanpy.pp.pca() to reduce the dataset's dimensionality while retaining key variance.

Determination of principal components and graph construction. To assess the optimal number of principal components for downstream analysis, the variance ratio was extracted from the PCA results, and an elbow plot was generated. The plot indicated that retaining at least 43 principal components captured the majority of variance in the dataset. A k-nearest neighbour (kNN) graph was then constructed using scanpy.pp.neighbors(), where each cell was connected to its 10 nearest neighbours (n_neighbors=10), and distances were computed using the first 50 principal components (n_pcs=50). Leiden clustering (scanpy.tl.leiden())

was subsequently applied to the graph to identify transcriptionally distinct cell clusters. A resolution parameter of 1.3 (resolution=1.3) was chosen, where higher values result in more granular clustering.

UMAP visualization and parameter optimization. UMAP was used for dimensionality reduction and visualization of cell clustering. The UMAP projection was initially computed using default parameters and minor adjustments were made to improve cluster separation.

Identification and removal of non-neuronal clusters. UMAP projections were examined with additional overlays of known marker genes to assess cluster identity. Glial marker genes (for example, *Aqp4*, *Slc1a3*, *Cx3cr1*, *P2ry12*, *Tmem119*, *Mbp*, *Olig1*, *Olig2* and *Pdgfra*) were visualized to identify clusters that are highly enriched in non-neuronal cell populations. As a validation step, neuronal markers (*Slc17a6, Slc17a7* and *Slc32a1*) were plotted to confirm that neuronal clusters did not overlap with glial-dominant populations. Following this assessment, clusters identified as non-neuronal were removed, and a new AnnData object was created containing only neuron-enriched cells. To ensure a clean dataset, all prior analyses, including PCA, UMAP and *k*NN graph computations, were reset (adata.uns entries such as X_umap, X_pca, neighbors, distances and connectivities were removed). This neuron-only dataset was then reprocessed from raw counts using the same normalization, log transformation and dimensionality reduction pipeline. PCA was recomputed, and the elbow plot was reassessed to determine the optimal number of retained principal components. The *k*NN graph, Leiden clustering and UMAP projection were recalculated to refine neuronal cluster assignments. Adjustments to clustering and visualization parameters were made iteratively to ensure biologically meaningful representation of neuronal subpopulations.

Visualization of gene expression. To visualize gene expression across clusters, UMAP plots were generated for genes of interest. Spatial expression patterns were examined using scanpy.pl.spatial(). Dot plots were generated using scanpy.pl.dotplot() to display gene expression levels and the proportion of expressing cells within each Leiden cluster.

To investigate the relationship between IEG expression and genes of interest, raw transcript counts were extracted from the primary data matrix (adata.X). A predefined threshold was applied to classify cells as either 'expressing' or 'non-expressing' *Npy1r*. *Fos* expression values were similarly extracted and stored. A separate DataFrame was created for ease of manipulation, where the median *Fos* expression of non-expressing cells was calculated to establish a baseline. This baseline was used to compute relative *Fos* expression (IEG_rel), enabling comparative analysis. A box plot was generated using Seaborn to visualize differences in *Fos* expression between *Npy1r* expressing and non-expressing cells within each Leiden cluster.

To identify marker genes for the Leiden clusters, sc.tl.rank_genes_groups() was used to perform differential expression analysis across clusters. The results were visualized using sc.pl.rank_genes_groups(), which ranks genes based on their log fold change (logFC) from highest to lowest. The top marker genes for each cluster were selected and presented in a dot plot to highlight representative gene expression patterns across clusters.

rAAV constructs

The following recombinant adeno-associated virus (rAAV) vectors were used: AAV5.hSyn.DIO.hM3D(Gq).mCherry (Addgene 44361 from B. Roth[54], titre: 2.1×10^{13} genome copies (GC) per ml), AAV8.hSyn.DIO.hM4D(Gi) (Addgene 44362 from B. Roth[54], titre: 2.2×10^{13} GC ml^{-1}), AAV2.FLEX.DTR.GFP (Addgene 124364 from E. Azim and T. Jessell[55], titre: 2.0×10^{13} GC ml^{-1}), AAV8.hSyn.fDIO.hm3D(Gq).mCherry.WPREpA (Addgene 154868 from U. Gether), AAV8.hSyn.DIO.mCherry (Addgene 50459 from B. Roth, titre: 3.6×10^{13} GC ml^{-1}), AAV1.Syn.Flex.GCaMP6s.WPRE.SV40 (Addgene 100845 from D. Kim and the GENIE project[56], titre: 4.2×10^{13} GC ml^{-1}), AAV1.hSynapsin1.axon.GCaMP6s (Addgene 111262 from L. Tian[57], titre: 4.1×10^{13} GC ml^{-1}), AAV1.syn.FLEX.splitTVA.EGFP.tTA (Addgene 100798 from I. Wickersham[58], titre: 1.2×10^{12} GC ml^{-1}), AAV1.TREtight.mTagBFP2.B19G (Addgene 100799 from I. Wickersham[58], titre: 1×10^{13} GC ml^{-1}), pSADdeltaG.mCherry (Addgene 32636 from E. Callaway[59], titre: 3.8×10^{12} GC ml^{-1}), AAV1.CBA.DO(FAS).GCaMP6s (Addgene plasmid 110135 from B. Sabatini[60], packaged by Vigene Biosciences, titre: 4.1×10^{13} GC ml^{-1}), AAV1.hSyn.Cre.WPRE.hGH (Addgene 105553 from J. M. Wilson, 2.5×10^{13} GC ml^{-1}), AAV1.CAG.FLEX.EGFP (Addgene 59331 from I. Wickersham), AAV1.hSyn.GRAB_NPY1.0 (Addgene 208676 from Y. Li[61] packaged by Neurotools), AAV1.CAG.GFP.U6.m.Npy1r.shRNA (Vector Biolabs), AAV1-EF1a-double floxed-hChR2(H134R)-EYFP-WPRE-HGHpA (Addgene 20298 from K. Deisseroth, titre: 2.1×10^{13} GC ml^{-1}) and AAV1.FLEX.tdTomato (Addgene 28306 from E. Boyden, titre: 3.1×10^{13} GC ml^{-1}). In the above vectors: hSyn refers to the human *SYN1* promoter; FLEX, Cre-dependent flip-excision switch; WPRE, woodchuck hepatitis virus response element; GCaMP, genetically encoded calcium indicator resulting from a fusion of GFP, M13 and calmodulin; DIO, double-floxed inverted orientation; fDIO, Flp-dependent double-floxed inverted orientation; hM4, human M4 muscarinic receptor; DTR, diphtheria toxin receptor; Ef1a, eukaryotic translation elongation factor 1α; SV40, simian virus 40; TVA, tumour virus receptor A; EGFP, enhanced green fluorescent protein; HGHpA, human growth hormone polyA.

Surgery

Intracerebral viral injections and fibre-optic and cannula placement. Viral injections and implants were performed as previously described[62]. In brief, mice were anaesthetized with isoflurane (3% induction, 1.5–3% maintenance), given ketoprofen (5 mg kg^{-1}, subcutaneous injection) and bupivacaine (2 mg kg^{-1}, subcutaneous injection) and placed into a stereotaxic frame (Stoelting, 51730). For viral injections, a craniotomy was performed above the injection site and virus injected at the following coordinates: lPBN: lambda −1.2 mm, midline ±1.4 mm, skull surface −3.3 mm; subparafascicular nucleus: bregma −2.3 mm, midline ±0.25 mm, skull surface −3.8 mm; vlPAG: bregma −4.5 mm, midline ± 0.2 mm, skull surface −2.7 and −2.55; arcuate: bregma −1.35 mm, midline ± 0.25 mm, skull surface −6.3 mm. Cre-dependent hM3D(Gq), hM4D(Gi), DTR, and mCherry were injected bilaterally (100–150 nl per side). Cre-dependent GCaMP6s, Cre-off GCamp6s, rabies helper viruses and rabies virus were injected unilaterally (150–200 nl). Rabies helper viruses were diluted, mixed, and injected in a single solution with a final dilution of 1:200 (TVA), 1:15 (G), and (for non-specific tracing only) 1:3 (Cre). Equal volumes of Cre-off GCaMP6s and Cre-dependent tdTomato were mixed and injected in a single solution. For fibre photometry experiments, an optic fibre (400 µm core, NA 0.66, Doric) was lowered 0.2 mm above the injection site and secured with metabond (Parkell) and dental cement. For pharmacological experiments, mice were implanted with 26-gauge guide cannulae (Plastics One) above the lPBN secured with metabond and dental cement. For miniscope imaging, Cre-dependent GCaMP6s (diluted, titre: 8×10^{12}) was injected unilaterally as described above. Then, a gradient index (GRIN) lens (0.6 mm diameter, 7.3 mm length, NA 0.5, Inscopix) was lowered 0.2 mm above the injection site and secured with metabond. A custom machined headbar was secured to the skull with super glue (Loctite Gel Control) and metabond, and then the whole implant was secured with black dental cement (Ortho-Jet). Kwik-Sil (WPI) was used to protect the lens before baseplate implantation. Two weeks later, the mouse was again anaesthetized and placed in the stereotaxic frame. A miniature microscope with a baseplate (UCLA Miniscope Project and OpenEphys) attached was lowered until the GRIN lens was in focus, and then slowly raised until cells were visible. The baseplate was secured using dental cement and the miniscope was detached. Mice were given at least two weeks for recovery and transgene expression. Expression and fibre placements were verified post-mortem.

Spinal cord injections. Spinal cord viral injections were performed as previously described[13]. Mice were anaesthetized with isoflurane

(3% induction, 1.5–3% maintenance) and given ketoprofen (5 mg kg^{-1}, subcutaneous injection) and bupivacaine (2 mg kg^{-1}, subcutaneous injection). An approximately 3 cm incision was made through the skin to expose vertebrae T12, L1, and L2. The muscle was gently removed and a laminectomy was performed to expose the spinal cord. The mouse was then placed in a stereotaxic frame to hold the spinal column in place. Cre-dependent axon GCaMP6s was injected unilaterally 0.5 mm lateral from the anterior spinal artery and 0.3 mm ventral from the dura mater. Two 500-nl injections were performed at the rostral and caudal ends of the exposed spinal cord. The skin was then sutured, and mice were given at least 3 weeks for recovery and viral expression.

Pain models

Spared nerve injury. Mice were anaesthetized with 5% isoflurane and anaesthesia was maintained at 2% isoflurane throughout surgery. The left hindlimb was shaved with electric trimmers and sterilized with 70% ethanol and povidone-iodine (Medline). An incision (2–3 cm) was made in the skin of the upper left hindleg and the muscle was spread to expose the branches of the sciatic nerve. The peroneal and tibial branches were ligated with silk suture (6-0) and transected. The skin was closed with 9-mm wound clips and topical triple antibiotic ointment (Neosporin) was applied to the wound. Wound clips were removed approximately 10 days post-surgery. Behavioural experiments began 14 days following surgery. Sham surgery involved the same surgical procedures, including exposure of the nerve but no ligation–transection[32].

Persistent inflammation. CFA (Sigma) was diluted 1:1 in saline and subcutaneously injected (30 µl) into the plantar surface of the paw of lightly anaesthetized mice (isoflurane). CFA experiments were performed between 1 and 4 days after CFA injection.

Hunger and thirst models

Food and water deprivation. For 24 h food deprivation, mice were placed in a clean cage with alpha dry bedding and ad libitum access to water, but no food, 24 h prior to experimentation. Ad libitum-fed control mice were also placed in a clean cage with alpha dry bedding but were given free access to chow. For 24 h water deprivation, the water bottle was removed from the home cage 24 h prior to experimentation. Body weight was measured before removing food or water and before experiments began.

Hypovolemic thirst. Mice were injected with PEG (30% subcutaneous injection) or saline and placed back in the home cage with the water bottle removed. They were placed in the behavioural chamber to habituate 45 min later. Formalin, von Frey and cold sensitivity tests began 60 min after PEG injection. To confirm that this dose induced thirst, a separate group of mice were injected and placed immediately into a new cage with an inverted 15 ml conical tube with a lick spout filled with water. Volume of water consumed was measured after 1 and 2 h and compared with saline injected controls.

Behavioural assays

DREADD-evoked food intake. Mice were habituated for at least 1 h to a cage with a lined floor (Kimberly-Clark, 75460) and ad libitum access to food and water. Following habituation, food was removed from the cage and mice were injected with clozapine-*N*-oxide (CNO, 1 mg kg^{-1} intraperitoneal) or saline and placed back in the cage with a weighed pellet of chow. Food was weighed after 1 h, accounting for crumbs.

Formalin test. Mice were habituated to handling and restraint before experiments began. Mice were placed in a clear enclosure for a 15 min habituation period. Then, 20 µl of 2% formalin (Sigma) were injected subcutaneously into the dorsal surface of the hindpaw. Tests were video-recorded and time spent licking during the 1 h assay was measured by scorers blinded to experimental condition. The time spent licking was grouped into 5 min bins, and the total time spent licking during the acute (0–5 min) and inflammatory (15–60 min) phase was calculated. In experiments where unilateral lPBN recordings or infusions took place, the contralateral paw was injected unless otherwise noted.

Effects of predator odour on formalin test. Mice were placed in the arena with a piece of absorbent paper taped to the side for a 15 min habituation period. Thirty microlitres of TMT (diluted 1:10 in PBS) or PBS was then pipetted onto the absorbent paper. 15 min later, formalin was injected into the paw as described above.

Effects of conditioned fear on formalin test. Mice were placed in a fear conditioning chamber (HABITEST modular behavioural test system, Coulbourn Instruments). After a 10 min habituation period, 1 shock (1 mA, 2 sec) was administered every 2 min over the course of 10 min (5 shocks total)[63]. 24 h later, mice were injected with formalin as described above. Mice were placed into the environment either immediately (to measure acute phase responding) or 20 min later (to measure inflammatory phase responding). Because conditioned fear extinguishes within 10 min, pain responding was only monitored in the fear-conditioned environment for 10 min. Mice were either placed in the shocked context (square chamber, grey walls and ceiling, shock rod flooring, cleaned with 70% ethanol) or an unshocked context (rounded chamber, black and white checkered walls and ceiling, cleaned with 5% acetic acid). Behaviour was video-recorded for 10 min following chamber entry. Freezing was scored automatically using ANY-Maze software (Stoelting, v7.08) and manually validated. Paw licking was scored manually.

Effects of lPBN Y1R neuron inhibition and AgRP neuron stimulation on formalin test. CNO (1 mg kg^{-1}) was injected intraperitoneally before the 15 min habituation period. The formalin test was then performed as described above.

von Frey test. Mice were habituated to small plexiglass chambers atop mesh flooring for 2 h per day for 3 days before experimentation and for 15 min before each test. The ascending method[64]: ten von Frey filaments (ranging from 0.04 g to 10 g) were used. Starting with the smallest von Frey filament and continuing in ascending order, each filament was applied to the plantar surface of the hindpaw until the filament bent. Each filament was tested 5 times with 1 min between each trial. A positive response was defined by one or more of the following: paw withdrawal, guarding, licking, shaking, or jumping. The number of positive responses was recorded for each filament, and the percentage of responses for each filament was calculated (# of withdrawal trials/total trials). Threshold was determined as the first filament at which the mouse had a positive response to 3 or more trials. The ascending method was used for CFA experiments. The up/down method[65]: logarithmically increasing calibrated von Frey filaments (Stoelting) ranging from 0.008 g to 6.0 g with a mean log interval of 0.41g were used for testing. Beginning with the 0.4 g filament, filaments were applied perpendicular to the surface of the lateral hindpaw with sufficient force to cause bending of the filament (~30°). A positive response was defined by one or more of the following: paw withdrawal, guarding, licking, shaking, or jumping. A positive response was followed by application of a lower gram force filament, while a negative response was followed by application of a higher gram force filament to calculate the 50% withdrawal threshold for each mouse. The up/down method was used for SNI experiments.

Acetone-induced cold sensitivity test. Acetone drop withdrawal testing was performed in the same Plexiglas chambers following von Frey testing. A syringe attached to PE-90 tubing with a tip flared to a 3.5 mm diameter was used to apply a 10 µl droplet of acetone to the lateral surface of the hindpaw. The length of time the animal spent lifting, shaking, and attending to the paw directly following droplet application was recorded, with a 30 s cutoff. Three trials were averaged for the final result[32].

Effects of lPBN Y1R neuron activation on von Frey and cold sensitivity tests. Compound 21 (1 mg kg^{-1}) was injected intraperitoneally 30 min before behavioural experiments.

Hot plate test. A cast iron plate with plexiglass walls was placed on a hot plate and heated to 52 °C. Mice were placed on the hot plate for 1 min (behaviour) or 20 s (fibre photometry). All sessions were video-recorded and the latencies to lick the forepaws, lick the hindpaws, and jump were scored along with the number of jumps during the test. Scoring was performed by experimenters blinded to experimental condition.
Effects of predator odour on hot plate test. Thirty microlitres of TMT was pipetted onto absorbent paper taped to the plexiglass wall. The mouse was then placed on the hot plate and responses were recorded as described above. The following data points were excluded: one mouse from each group did not lick their forepaws during the assay and two PBS mice and one TMT mouse jumped onto the paper for several seconds and therefore their jump score was excluded.
Effects of food deprivation on hot plate test. Naive mice were placed on the hot plate as described above for a habituation trial. Food was removed from half the cages as described above and the assay was run again the next day. Food was then returned to all mice.
Effects of hypothalamic AGRP or NPY neuron stimulation and Y1R neuron inhibition on hot plate test. Mice expressing DREADDs in the arcuate or PBN were placed on the hot plate as described above for a habituation trial. At least 2 days later, half the mice were injected with saline and half with CNO (1 mg kg^{-1}, intraperitoneal) followed by the hot plate test 30 min later. For NPY neuron stimulation, the experiment was then counter balanced three days later.

Inflammation-induced sensitization. An alligator clip (UQ003, Uniquers) was applied to the ventral surface of the paw as previously described to establish the baseline neural response to mechanical pain[38]. At least two days later, CFA was injected into the plantar surface of the paw as described above. The neural response to clipping the paw was recorded 48 h later in ad libitum-fed mice. Food was then removed from the cage. The neural response to clipping the paw was measured again, 24 h later, in food-deprived mice. Paw size was measured daily using a plethysmometer (Stoelting, 57140) to ensure that any effects were not due to changes in inflammation levels.

Conditioned place avoidance. Two-sided apparatuses were used with distinct visual (black versus white walls) and textural (flooring: plastic versus soft textural side of Kimtech bench-top protector) cues. A neutral middle zone to shuttle between sides was maintained and the chamber was equipped with an overhead camera to track mouse position. Mice were habituated to the apparatus and a pre-conditioning preference was determined over four 30 min sessions via ANY-maze software (Stoelting). Conditioning was performed daily for four days. During conditioning, mice expressing hM3D(Gq) or control virus in lPBN Y1R neurons were injected with saline (intraperitoneally) and placed into their non-preferred side for 30 min in the morning and injected with CNO (1 mg kg^{-1}, intraperitoneal) and placed into their preferred side for 30 min in the afternoon. To test post-conditioning preference, mice were again placed in the chamber with free access to both sides for two 30 min sessions, and their activity was tracked. The percentage of time spent in the CNO-paired side of the chamber before and after conditioning was calculated and averaged to determine the shift in preference caused by activation of lPBN Y1R neurons.

Innate fear assay. Mice were placed in a chamber with absorbent paper taped to the floor on one side and their activity was tracked by an overhead camera. After a 15 min baseline period, 30 µl of TMT was pipetted onto the paper and mice were left in the chamber for another 15 min. Using ANY-maze, we quantified the number of entries into and time spent in the 'odour zone', which was defined as the area around the absorbent paper with a circumference of the mouse's body length (excluding the tail).

Conditioned taste aversion. Mice were habituated to cages with lined flooring for at least 1 h and food was removed from the home cage for 24 h as described above. On day 1, mice were given 0.5 g of strawberry or orange Jell-O. Five minutes after their first bite, mice were injected with either saline (control) or LiCl (to induce aversion, 125 mg kg^{-1}, intraperitoneal) and allowed to finish the Jell-O. Mice were then returned to their home cages with ad libitum access to chow and water. The next day, food was again removed from the cage. On the third day, mice were presented with 1.5 g of the same flavour of Jell-O they had on day 1, and the weight of the remaining Jell-O was recorded at 30 min and 60 min.

Open field assay. Mice were habituated to the open field area (400 mm^2) for 15 min. Mice were then tracked by ANY-maze software (60 min for ablation experiments, 30 min for all other experiments). The centre was defined as the middle third of the arena.

Drugs and pharmacology

Formalin (2%, Sigma), PEG (30%, average relative molecular mass 1,500, Acros Organics), CFA (50%, Sigma), LiCl (12.5 mg ml^{-1}, Sigma), CNO (0.1 mg ml^{-1}, Tocris), ghrelin (60 µg ml^{-1}) and diphtheria toxin (0.5 mg ml^{-1}, List Labs) were diluted in normal saline. Formalin and CFA were injected subcutaneously in the hindpaw at a volume of 20 µl (formalin) or 30 µl (CFA). PEG was injected subcutaneously at a volume of 20 µl per g body weight. Ghrelin, LiCl and CNO were injected intraperitoneally at a volume of 10 µl per g body weight. Diphtheria toxin was injected intramuscularly at a volume of 5 µl per g body weight. Mice received 3 diphtheria toxin injections under light isoflurane anaesthesia with 48 h between injections.

Effects of lPBN NPY Y1 receptor antagonist on the analgesic effects of competing threats. For all experiments, mice were habituated to handling and infusion procedures. BIBO 3304 (Tocris) was dissolved in DMSO and frozen in aliquots. Aliquots were thawed and diluted 1:1 in artificial cerebrospinal fluid (aCSF) before each experiment. Three micrograms of BIBO 3304 or vehicle (1:1 solution of DMSO and aCSF) was microinjected (100 nl) with a Hamilton syringe attached to an internal cannula (Plastics One) and microlitre syringe pump (PHD Ultra, Harvard Apparatus) into the lPBN of mice immediately before the formalin test, von Frey test, or acetone test (see above).

Effects of lPBN NPY on persistent inflammatory and neuropathic pain. Neuropeptide Y (NPY, Tocris) was dissolved in saline and frozen in aliquots. Aliquots were thawed and diluted 1:1 in aCSF before each experiment. NPY (0.1 µg in 100 nl) or vehicle (aCSF, 100 nl) was microinjected with a Hamilton syringe attached to an internal cannula as described above. Mice were then placed on the caged floor and allowed to habituate for 15 min before the von Frey or acetone tests began.

Calcium imaging

Fibre photometry. Dual-wavelength fibre photometry was performed as described[66,67]. Two excitation wavelengths (470 nm and 405 nm) were delivered through fibre-coupled LEDs (Thorlabs, M470F3 and M405F1) modulated at 211 and 566 Hz by a real-time amplifier (Tucker-Davis Technologies, RZ5P or RZ10x). Excitation lights were filtered and combined by a fluorescence minicube (Doric). The light was delivered through a 400 µm core, 0.57 NA low autofluorescence optical fibre (Doric, MFP_400/430/1100-0.57_1m_FC-MF2.5_LAF) to the implanted fibre (Doric, MFC_400/430-0.66_4.0mm_MF2.5_FLT). The fibres were secured by a clamp (Thorlabs, ADAF2). LED power was set between 20 and 40 µW emitted from the fibre tip to minimize bleaching. GCaMP fluorescence was collected from the same optical fibre and focused

onto a femtowatt receiver (Newport, Model 2151, gain set to DC LOW). Fluorescence was sampled at 1,017 Hz and demodulated by the processor. LEDs were externally controlled by Synapse (Tucker-Davis Technology) and synchronized cameras (Ailipu Technology) were used to video record mice during experiments. Mice were habituated to tethering before experiments began. A 5 min baseline before any stimulus was given was recorded and used to normalize subsequent changes in fluorescence.

Fibre photometry after SNI. Three weeks following fibre-optic implant surgeries, animals were habituated to Plexiglas chambers, elevated wire mesh, and patch cable attachment for 1 h each 2 days prior to experiments. On the day of experimentation, animals were habituated in Plexiglas chambers on elevated wire mesh for 1 h before having patch cables attached to the implanted fibre-optics and habituating for an additional 30 min with the experimenter in the room. Baseline recordings were performed to innocuous and noxious stimuli according to the following paradigm: 0.07 g von Frey filament, 1.0 g von Frey filament, acetone, and blunted pin prick. Calcium transients were collected continuously (FP3002, Neurophotometrics) during the stimulation protocol. Each stimulus was applied to the lateral surface of the left hindpaw three times 2 min apart, and all three responses were averaged to represent the animal's response to that stimulus. Following baseline recordings, animals underwent SNI surgery in the left hindlimb to induce neuropathic pain. The fibre photometry protocol was repeated 21 days after SNI surgery.

Fibre photometry analysis. Data were exported to MATLAB (MathWorks) from Synapse using scripts provided by Tucker-Davis Technology. Custom MATLAB scripts were used to independently normalize the demodulated 470 nm and 405 nm signals. $\Delta F/F$ was calculated $(F - F_{\text{baseline}})/F_{\text{baseline}}$, with F_{baseline} being the median of the 300 s before the stimulus. *z*-Scores were used in cases where multiple days separated within subject recordings in order to correct for changes in signal strength over time. Data were down-sampled to 1 Hz. Subsequent plotting and analyses were performed in MATLAB and Prism 10 (GraphPad). Mean $\Delta F/F$ was calculated by integrating $\Delta F/F$ over a period of time after the stimulus and then dividing by the integration time. Maximum $\Delta F/F$ during hot plate recordings were calculated by finding the maximum $\Delta F/F$ value of each mouse during the hot plate window. Recordings comparing paw licking during formalin and sucrose application to the paw were smooth with a 5 s sliding window for visualization only.

SNI fibre photometry analysis. Custom MATLAB scripts were used to normalize the GCamp6s (470 nm) signal to the isosbestic signal (405 nm), controlling for motion artefacts as well as photobleaching. The change in fluorescence ($\Delta F/F$) was calculated by subtracting the GCamp6s signal during stimulation from the average GCamp6s signal over the 10 s directly prior to stimulation. Mean and maximum $\Delta F/F$ were calculated as described above.

Fitting fibre photometry signal from behaviour. To fit the photometry signal to licking behaviour, we denote the $\Delta F/F$ photometry signal as $\varphi(t)$. First, we subtract the value such that 1% of the signal $\varphi(t)$ is negative and fit the behaviour of each individual mouse to its photometry recording by minimizing the sum of squares:

$$\min_{A,\tau} \sum_{t=0}^{T} \left(\varphi(t) - Ae^{-\frac{t}{\tau}} * L(t)\right)^2.$$

L is the licking behaviour, a binary sequence, and it is convolved with an exponential kernel. We find the parameters by looping over time constant τ, and utilize least squares to find A. To constrain τ, we choose the time constant that gives the highest average Pearson correlation on all other mice in the same experimental condition. We report the ensuing Pearson correlation coefficients, indicating the extent to which the behaviour co-varies with the bulk calcium signal. We model the slow component, denoted by $s(t)$, in the photometry signal by two Gaussian curves:

$$s(t) = a_1 e^{-(a_2-t)^2/2a_3^2} + a_4 e^{-(a_5-t)^2/2a_6^2}.$$

We fit the six parameters to the lower envelope of the calcium signal using MATLAB functions envelope and fmincon. Specifically, we subtract the lower envelope using argument peak and a smoothing of 30 s. We do this to model the slow baseline signal on top of which the fast behavioural fluctuations ride. We then fit the behavioural sequence $L(t)$ to the difference between the photometry signal and the slow component, using the earlier described method:

$$\min_{A,\tau} \sum_{t=0}^{T} \left(\varphi(t) - s(t) - Ae^{-\frac{t}{\tau}} * L(t)\right)^2.$$

Microendoscopy. A miniature microscope (Miniscope Project, UCLA) was used to image individual lPBN Y1R neurons. Mice were habituated to handling and the attachment of the camera by the experimenter for at least one week prior to experiments. Open-source software (Miniscope Project, UCLA) was used to acquire video from the miniscope and a behavioural camera. Optimal LED power, gain, and focal plane were determined for each mouse that provided the clearest view and dynamic range of the most cells. Recoded timestamps were used to synchronized frames across data streams. For the formalin test, a 5 min baseline recording was obtained. Formalin was then injected as described above, and recording commenced for 1 h. To avoid bleaching, the LED was shut off for 1 min every 5 min.

Microendoscopy analysis. Calcium imaging data were analysed using custom code based on the open-source analysis pipeline Minian[68]. In brief, videos were preprocessed to remove glow artefacts and background signal and correct for motion using both rigid and non-rigid motion correction. Then, units were detected and traces extracted using the CNMF algorithm. Two spatial and two temporal updates were used to identify cells based on spatial footprints and temporal dynamics. Each identified unit was either confirmed or rejected by the experimenter. The calcium traces and behavioural videos were loaded into the open-source MATLAB GUI Bento for behavioural annotation[69]. We annotated for paw-licking, face-grooming, rearing and walking during the first 5 min before the formalin injection, and during the 60 min after injection. The Pearson correlation between the behaviours and each individual neuron was computed, after *z*-scoring the neurons using the mean and s.d. of their baseline activity. A neuron was classified as a 'lick on' neuron when the correlation was significantly larger than expected—that is, when the correlation was larger than 97.5% of all correlations obtained by reshuffling the paw-licking bouts 3,000 times. We classified neurons as correlated with 'other behaviour' in the same manner, using the annotations for rearing, grooming and walking. To identify neurons modulated by the pain state, we take the activity of neurons during which no annotated behaviour occurs and compare it to their baseline activity. A neuron is then classified as a 'pain on' neuron when it is: (1) unclassified by a behaviour; and (2) the s.d. of activity after formalin injection was significantly larger than the s.d. of activity before—that is, the difference was larger than 97.5% of all differences obtained by reshuffling the time series of the neuron 3,000 times. Conversely, a neuron is a 'pain off' neuron when it is: (1) unclassified by a behaviour; and (2) the median activity is significantly lower after the injection.

Model of pain behaviour

To model the control of pain-evoked licking behaviour under competing needs, we assume that animals aim to reduce experienced pain while also minimizing effort expended[70]. Animals show multiple behaviours in response to acute and chronic pain, including active coping methods like wound licking (an instinctive behaviour that cleans and disinfects wounds[71]) and more passive strategies such as paw guarding to reduce allodynia; for the purpose of comparison to experimental data, this model focuses only on wound licking behaviour. Excess wound licking

leads to risk of lesion formation and infection[72], and the act of wound licking costs energy and saliva and comes with an 'opportunity cost', in that it prevents the animal from pursuing other activities required for survival. 'Effort' in this model may therefore be taken as an abstract variable that encapsulates the overall negative consequences of licking more than is necessary to reduce pain.

We therefore posit a minimal reinforcement learning model of pain-related behaviour consisting of two state variables and one action variable, where the action is either licking ($L = 1$) or not licking ($L = 0$), and the state variables are 'pain' (P) and 'effort' (E). Mathematically, the model aims to maximize the sum of discounted future rewards. However, because there are no traditional rewards, we define the reward in terms of deviations from a homeostatic setpoint, inspired by Keramati & Gutkin[73]:

$$D(t) = P^2(t) + \alpha E^2(t)$$

where $D(t)$ is the drive at time t, assuming zero pain and effort as the optimal homeostatic setpoint. We define the reward $R(t)$, to be optimized, as the difference in drive:

$$\max \sum_{t=0}^{T} \gamma^t R(t) = \max \sum_{t=0}^{T} \gamma^t (D(t) - D(t+1))$$

The parameter γ is smaller than 1 and determines temporal discounting, T is the total simulation time. The parameter α may set the relative cost of pain versus effort but is here chosen to be one. Given this definition, a behavioural policy is defined as a mapping from the two-dimensional state of the system ($P(t)$, $E(t)$) to the action $L(t)$ (whether to lick).

Before finding this behavioural policy, we must first define how the two state variables—pain and effort—are modified by the licking action L and by ascending nociceptive input in the assay.

We first consider the effort state variable, denoted E. Effort is exerted with each lick, and gradually recovers after a lick bout is over; it therefore takes the form of an exponential filter of the licking:

$$E(t) = A e^{-t/\tau_E} * L(t)$$

where $*$ denotes the convolution operation, τ_E is the time constant of exponential smoothing and A is the scaling factor. As an abstract state variable, the units of E are somewhat arbitrary. Therefore, to select the values of τ_E and A, we referenced the range of values found for exponential and scaling terms when fitting a linear filter of licking behaviour and slow input to the photometry data. This gave us values of $\tau_E = 4$ sec and $A = 0.07$.

We next considered the pain state variable, denoted P. In designing the form of P, we noted that a linear model could not reproduce the finding that competing need states inhibit inflammatory but not acute pain, unless we either: (1) assume these two forms of pain come from different sources, one of which is independent of regulation by NPY; or (2) introduce a nonlinearity in the relationship between ascending pain and the pain state. To test whether the latter model of a single pain source would be sufficient to account for observed behaviour, we here introduced a nonlinearity into P, designing it to be a saturating integral of the ascending nociceptive input from the formalin injection:

$$x(t+1) = x(t) + \frac{1}{\tau_P}((P(t) - x(t)) + P_{\text{input}}(t) - wL(t))$$

$$P(t) = f(x(t))$$

where the subscript denotes time, τ_P is an integration time constant, w is the degree to which licking affects the pain state, and P_{input} is ascending nociceptive input. Like E, P is an abstract quantity with arbitrary units; thus, we set our integration time constant and licking weight to ensure that P and E were of comparable magnitude: this gave us $w = 0.035$ and $\tau_P = 5$ sec. For the case of formalin injection, P_{input} was modelled as the sum of two Gaussians, such that P resembles the slow signal in the photometry (see 'Fibre photometry analysis' and Extended Data Fig. 10). $f(\cdot)$ is a nonlinearity that keeps the value of P between a minimal and maximal level (Extended Data Fig. 10), $\{f(x) = 0$ if $x < 0$, $f(x) = x$ if $x < K$ and $f(x) = K + \tanh(10x)/10$ if $x > K\}$. Here, the value K is chosen to match model output to mice ad libitum licking behaviour, $K = 0.35$. Thus, x is an intervening variable shaped by: (1) the effect of licking; (2) the ascending pain input; and (3) the difference between x and P, which is positive when $x < 0$, 0 in the linear portion of f, and negative when $x > K$. The difference term therefore has the effect of a restoring force that reduces excursions outside the linear regime of f.

Having established E and P, we can next learn a behavioural policy that maximizes reward, that is, maximizes $\sum_{t=0}^{T} \gamma^t (D(t) - D(t+1))$. We parametrized the model's behavioural policy by a feedforward network: $L(t) = g_\theta(P(t), E(t))$, and used Q-learning[74] to find the network parameters θ. The feedforward network is all-to-all connected, with 6 hidden layers of 128 rectified linear units. To avoid having to model the duration of lick bouts, when the policy generates a lick, the duration is sampled from the empirical distribution of lick bout durations found in the data. We give more details and vary multiple aspects of the model in the Supplementary Information. In short, we verify that a linearization of the pain dynamics or adding delay to the licking feedback, $-wL(t-d)$, does not affect our results qualitatively.

We study the effect of competing needs in the model by modulating the three parts of the model as shown in Fig. 4a, denoting the modulation by a constant NPY > 0. During training, 25% of trials were randomly selected to include the modulation and in other trials we set NPY = 0. We verified that selecting 50% of trials at random did not change our results (Supplementary Note). Each of the three parts is manipula ted in two ways.

Modulation I: modelling a change in the integration of pain input. We tested two alternative ways of manipulating integration of nociceptive input:

Manipulation 1.

$$x(t+1) = x(t) + \frac{1}{\tau_P}(P(t) - x(t) + P_{\text{input}}(t) - wL(t) - \text{NPY})$$

Manipulation 2.

$$x(t+1) = x(t) + \frac{1}{\tau_P}(P(t) - x(t) + P_{\text{input}}(t) - wL(t) - \text{NPY} \cdot x(t)).$$

We find that this model can reproduce the experimentally observed reduction in licking when we set NPY = 0.001 and NPY = 0.0075, respectively.

Modulation II: modelling an increase in the effort cost of licking. We tested two alternative ways of manipulating the effort cost of licking, either by doubling the time constant τ_E or doubling the amplitude A in the equations for the dynamics of E:

$$\text{Manipulation 1. } E(t) = A e^{-\frac{t}{\tau_E + \text{NPY}}} * L(t)$$

$$\text{Manipulation 2. } E(t) = (A + \text{NPY}) e^{-\frac{t}{\tau_E}} * L(t).$$

Modulation III: changing the behavioural policy. We tested two alternative ways of incorporating the third axis to the behavioural policy, introducing NPY as a scaling of either the pain variable or the effort variable in the reward function:

$$\text{Manipulation 1. } D(t) = f(x(t) - \text{NPY})^2 + \alpha E^2(t)$$

Manipulation 2. $D(t) = P^2(t) + \alpha(1 + \mathrm{NPY})E^2(t)$.

Here, NPY = 0.1 and NPY = 0.2 respectively. In this revised policy, NPY is given as an additional input to the feedforward network: $L(t) = g_\theta(P(t), E(t), \mathrm{NPY})$, and we assume that its value remains constant during the time of the experiment.

Only the modulation to pain state integration leads to behavioural and state timeseries consistent with the data. We show the first manipulation of each modulation in Fig. 4, while the second manipulation is shown in Extended Data Fig. 10.

Histology

Verification of viral expression and fibre placement. Mice were transcardially perfused with 0.1 M PBS followed by 4% paraformaldehyde (PFA). Brains were removed and post-fixed for 4 h in PFA and then washed overnight in PBS. Coronal brain sections were cut (150–200 µm sections) on a vibratome, washed twice with PBS, and mounted and coverslipped with Fluorogel. Epifluorescence images were taken on a Leica stereoscope to verify fibre and cannula placements and viral expression. In rare cases (1 Y1R, 2 Vglut2 and 1 non-Y1R) animals died before fibre locations could be determined.

Immunohistochemistry. Brain sections were incubated overnight at 4 °C with primary antibodies diluted in PBS, 1% BSA and 0.1% Triton X-100. Antibodies used: goat anti-AgRP (1:2,500, Neuromics, GT15023), rabbit anti-FOS (1:1,500, Cell Signaling Technology, 2250) guinea pig anti-RFP (1:10,000)[75] and rabbit anti-GFP (1:5,000, Invitrogen, A-11122). Sections were washed 3 times and incubated with species appropriate and minimally cross-reactive fluorophore-conjugated secondary antibodies (Donkey anti-Goat Cy5 AffiniPure 705-175-147, Donkey anti-Rabbit Cy5 Affinipure 711-175-152, Donkey anti-Guinea Pig Cy3 AffiniPure 706-165-148, and Donkey anti-Rabbit Alex Fluor 488 AffiniPure 711-545-152, all 1:500, Jackson ImmunoResearch) for 2 h at room temperature. Sections were washed twice with PBS and mounted and coverslipped with Fluorogel. Confocal images were taken on a Leica DM6 Upright Microscope using a 20× or 63× objective using LASX (v.3.7.4) software.

Tissue clearing and light sheet microscopy. Light sheet microscopy was used to visualize lPBN Y1R projections. Tissue clearing and light sheet microscopy were performed by LifeCanvas Technologies. Samples were preserved using SHIELD reagents (LifeCanvas Technologies) according to the manufacturer's instructions[76], and were then delipidated using Clear+ delipidation reagents (LifeCanvas Technologies). Samples were index matched by incubating in 50% EasyIndex (refractive index = 1.52, LifeCanvas Technologies) overnight at 37 °C followed by incubation in 100% EasyIndex for 1 day. The samples were then imaged using a SmartSPIM axially swept light sheet microscope using a 3.6× (0.2 NA) objective (LifeCanvas Technologies).

Fluorescence in situ hybridization. Brains were post-fixed overnight and then transferred to a 30% sucrose solution for 48 h. Brains were then frozen in OCT compound (Fisher Scientific) and stored at −80 °C. Brains were sectioned at 12–15 µm in a cryostat onto Superfrost Plus slides (Fisher Scientific) and stored at −80 °C until use. Fluorescence in situ hybridization (FISH) was performed according to manufacturer instructions (RNAscope fixed-frozen tissue, ACD) using the following probes: Mm-Npy1r (427021), Mm-Penk (318761), Mm-Pdyn (318771), Mm-Tacr1 (428781) and Mm-Calca (578771).

FISH imaging. Sections were imaged on a slide scanning light microscope (Keyence). Exposure times were kept consistent across all sections in an experiment. Tile scans were collected of the entire lPBN using a 40× objective and stitched using BZ X800 Analyzer Software (Keyence).

FISH analysis. FISH analyses were performed in ImageJ (NIH, v.1.53 f). ROIs were drawn manually by circling all DAPI-positive areas in the lPBN. Then, in each channel, the intensity of five representative 'background' regions without any fluorescent labelling and the intensity of 20 single 'dots' representing an mRNA transcript were measured. The approximate dot number per cell was calculated by dividing the total intensity of a DAPI-labelled ROI minus the background by the average dot intensity. A cell was considered positive if it had an estimated dot number greater than or equal to 1.

Slice electrophysiology

Slice preparation. Animals were deeply anaesthetized with isoflurane and rapidly decapitated. Following brain dissection, the brain was submerged in oxygenated ice cold *N*-methyl-D-glucamine (NMDG) recovery solution (in mM: 2.5 KCl, 20 HEPES, 1.2 NaH_2PO_4, 25 glucose, 93 NMDG, 30 $NaHCO_3$, 5.0 Sodium ascorbate, 3.0 sodium pyruvate, 10 $MgCl_2$ and 0.5 CaCl-$2H_20$; 300–305 mOsm). The brain was blocked and coronal slices were obtained using a Campden Instruments 7000 smz-2 vibrotome in ice-cold, oxygenated NMDG solution. After sectioning, slices were transferred to a recovery holding chamber containing 32 °C NMDG solution. Slices recovered for 10 min before being transferred to a holding chamber containing room temperature aCSF (in mM: 119 NaCl, 2.5 KCl, 1.3 $MgCl_2.6H_2O$, 2.5 $CaCl_2.2H_2O$, 1 $NaH_2PO_4.H_2O$, 26.2 $NaHCO_3$ and 11 glucose; 287–295 mOsm). Slices were allowed to recover for an additional 1 h before recording.

Electrophysiology. Electrophysiology experiments were performed on a Scientifica Slicescope Pro system. Recordings were acquired using a Multiclamp 700B amplifier and a Digidata 1550B digitizer. Data was filtered at 2 kHz and digitized at 10 kHz. Slices were superfused with oxygenated 30 °C aCSF. Recordings took place in the lPBN dorsal to the superior cerebellar peduncle and ventral to the ventral spinocerebellar tract. Y1R-expressing neurons were identified by fluorescent reporter and patched with 3–6 MΩ pipettes prepared with a Sutter Instrument P-97 pipette puller. For synaptic connectivity experiments, these pipettes contained a $CsMeSO_3$ based internal solution (in mM: 120 $CsMeSO_3$, 15 CsCl, 8 NaCl, 10 HEPES, 0.2 EGTA, 5 TEA-Cl, 4 Mg_2-ATP, 0.3 Na_2-GTP, 0.1 Spermine tetrahydrochloride, 5 QX-314 bromide, 5 phosphocreatine disodium salt; pH 7.4, 290 mOsm). Channelrhodopsin-mediated optically evoked post synaptic potentials were generated using 0.3 ms 490 nm light pulses from a CoolLED pE-4000 illumination system. For CFA sEPSC recordings and DREADD validation recordings, pipettes were filled with a potassium gluconate-based internal solution (in mM: 135 potassium gluconate, 10 NaCl, 2 $MgCl_2$, 0.16 $CaCl_2$, 10 HEPES, 0.5 EGTA, 4 Mg_2-ATP, 0.4 Na_2-GTP. Membrane potential was clamped at −60 mV and cells were allowed to equilibrate for 5 min following establishment of the whole-cell configuration. For CFA recordings, animals were sacrificed 24 h post 30 µl 1:1 CFA: saline paw injection. sEPSCs were recorded in the voltage clamp configuration for 3 min and analysed in Clampfit 11 with a stringent best-fit template. For DREADD validation recordings, cells were injected with sufficient current in the current clamp configuration to maintain their membrane potential at −50 mV for hM4D(Gi) recordings. Following a 3-min baseline, 1 µM of CNO was bath-applied.

Statistics and reproducibility

Data were expressed as mean ± s.e.m. in figures and text unless noted otherwise. Paired or unpaired two-tailed *t*-tests, Wilcoxon signed-rank tests, and Pearson regressions were performed as appropriate. One-way, two-way and three-way ANOVA were used to make comparisons across more than two groups. The Shapiro–Wilk test was used to test the normality of residuals. Equal variance was not assumed, and Welch's corrections or Greenhouse–Geisser corrections were applied. To compare

Pearson's correlations between groups, Fisher's *z*-transformation was applied to *r* values before conducting *t*-tests. One statistical outlier was identified using the ROUT method and was removed from Extended Data Fig. 8q (TMT). In Fig. 1g, samples with fewer than 10 cells that met the criteria were excluded (Cluster N5 *Npy1r*+, 1 excluded; Cluster N8 *Npy1r*+, 6 excluded; Cluster N9 *Npy1r*+, 3 excluded; Cluster N10 *Npy1r*+, 2 excluded). Clusters N11–N14 were excluded owing to low cell counts in both groups. Micrographs are representative of four mice (Fig. 5h), three mice (Extended Data Fig. 2d), four mice (Extended Data Fig. 3c, control), five mice (Extended Data Fig. 3c, ablated), two mice (Extended Data Fig. 5b), three mice (Extended Data Fig. 8b), six mice (Extended Data Fig. 8d–i), two mice (Extended Data Fig. 8w) and three mice (Extended Data Fig. 9a). All statistics were performed using Prism 10 (GraphPad). Test, statistics, significance levels and sample sizes for each experiment are listed in Supplementary Tables 1–3. Not significant, $P > 0.05$, *t*-tests and post hoc comparisons: $^{*}P < 0.05$, $^{**}P < 0.01$, $^{***}P < 0.001$; interaction: $^{\dagger}P < 0.05$, $^{\dagger\dagger}P < 0.01$, $^{\dagger\dagger\dagger}P < 0.001$; main effect (group, condition or drug): $^{\#}P < 0.05$, $^{\#\#}P < 0.01$, $^{\#\#\#}P < 0.001$.

Reporting summary

Further information on research design is available in the Nature Portfolio Reporting Summary linked to this article.

Data availability

The spatial transcriptomic dataset generated in this study has been deposited in the NCBI Gene Expression Omnibus (GEO) and are accessible through the GEO Series accession number GSE301435. Source data are provided with this paper.

Code availability

Custom code generated to analyse data and build the pain model are accessible at https://github.com/KennedyNeuro/parabrachial-hub-2025.

46. Padilla, S. L. et al. Agouti-related peptide neural circuits mediate adaptive behaviors in the starved state. *Nat. Neurosci.* **19**, 734–741 (2016).
47. Daigle, T. L. et al. A suite of transgenic driver and reporter mouse lines with enhanced brain-cell-type targeting and functionality. *Cell* **174**, 465–480.e22 (2018).
48. Krashes, M. J. et al. A novel excitatory paraventricular nucleus to AgRP neuron circuit that drives hunger. *Nature* **507**, 238–242 (2014).
49. Vong, L. et al. Leptin action on GABAergic neurons prevents obesity and reduces inhibitory tone to POMC neurons. *Neuron* **71**, 142–154 (2011).
50. Loh, K. et al. Inhibition of Y1 receptor signaling improves islet transplant outcome. *Nat. Commun.* **8**, 490 (2017).
51. Sieber, M. A. et al. Lbx1 acts as a selector gene in the fate determination of somatosensory and viscerosensory relay neurons in the hindbrain. *J. Neurosci.* **27**, 4902–4909 (2007).
52. Milstein, A. D. et al. Inhibitory gating of input comparison in the CA1 microcircuit. *Neuron* **87**, 1274–1289 (2015).
53. Tong, Q., Ye, C.-P., Jones, J. E., Elmquist, J. K. & Lowell, B. B. Synaptic release of GABA by AgRP neurons is required for normal regulation of energy balance. *Nat. Neurosci.* **11**, 998–1000 (2008).
54. Krashes, M. J. et al. Rapid, reversible activation of AgRP neurons drives feeding behavior in mice. *J. Clin. Invest.* **121**, 1424–1428 (2011).
55. Azim, E., Jiang, J., Alstermark, B. & Jessell, T. M. Skilled reaching relies on a V2a propriospinal internal copy circuit. *Nature* **508**, 357–363 (2014).
56. Chen, T.-W. et al. Ultrasensitive fluorescent proteins for imaging neuronal activity. *Nature* **499**, 295–300 (2013).
57. Broussard, G. J. et al. In vivo measurement of afferent activity with axon-specific calcium imaging. *Nat. Neurosci.* **21**, 1272–1280 (2018).
58. Liu, K. et al. Lhx6-positive GABA-releasing neurons of the zona incerta promote sleep. *Nature* **548**, 582–587 (2017).
59. Osakada, F. et al. New rabies virus variants for monitoring and manipulating activity and gene expression in defined neural circuits. *Neuron* **71**, 617–631 (2011).
60. Markowitz, J. E. et al. The striatum organizes 3D behavior via moment-to-moment action selection. *Cell* **174**, 44–58.e17 (2018).
61. Wang, H. et al. A tool kit of highly selective and sensitive genetically encoded neuropeptide sensors. *Science* **382**, eabq8173 (2023).
62. Low, A. Y. T. et al. Reverse-translational identification of a cerebellar satiation network. *Nature* **600**, 269–273 (2021).
63. Penzo, M. A. et al. The paraventricular thalamus controls a central amygdala fear circuit. *Nature* **519**, 455–459 (2015).
64. Kim, S. H. & Chung, J. M. An experimental model for peripheral neuropathy produced by segmental spinal nerve ligation in the rat. *Pain* **50**, 355–363 (1992).
65. Chaplan, S. R., Bach, F. W., Pogrel, J. W., Chung, J. M. & Yaksh, T. L. Quantitative assessment of tactile allodynia in the rat paw. *J. Neurosci. Methods* **53**, 55–63 (1994).
66. Su, Z., Alhadeff, A. L. & Betley, J. N. Nutritive, post-ingestive signals are the primary regulators of AgRP neuron activity. *Cell Rep.* **21**, 2724–2736 (2017).
67. Goldstein, N., Carty, J. R. E. & Betley, J. N. Specificity of varenicline in blocking mesolimbic circuit activation to natural and drug rewards. *Neuroscience* **483**, 40–51 (2022).
68. Dong, Z. et al. Minian, an open-source miniscope analysis pipeline. *eLife* **11**, e70661 (2022).
69. Segalin, C. et al. The Mouse Action Recognition System (MARS) software pipeline for automated analysis of social behaviors in mice. *eLife* **10**, e63720 (2021).
70. Seymour, B., Crook, R. J. & Chen, Z. S. Post-injury pain and behaviour: a control theory perspective. *Nat. Rev. Neurosci.* **24**, 378–392 (2023).
71. Ashcroft, G. S. et al. Secretory leukocyte protease inhibitor mediates non-redundant functions necessary for normal wound healing. *Nat. Med.* **6**, 1147–1153 (2000).
72. Weil, H.-P., Fischer-Brügge, U. & Koch, P. Potential hazard of wound licking. *N. Engl. J. Med.* **346**, 1336–1336 (2002).
73. Keramati, M. & Gutkin, B. Homeostatic reinforcement learning for integrating reward collection and physiological stability. *eLife* **3**, e04811 (2014).
74. Mnih, V. et al. Human-level control through deep reinforcement learning. *Nature* **518**, 529–533 (2015).
75. Betley, J. N., Cao, Z. F. H., Ritola, K. D. & Sternson, S. M. Parallel, redundant circuit organization for homeostatic control of feeding behavior. *Cell* **155**, 1337–1350 (2013).
76. Park, Y.-G. et al. Protection of tissue physicochemical properties using polyfunctional crosslinkers. *Nat. Biotechnol.* **37**, 73–83 (2019).

Acknowledgements The authors thank the Betley laboratory for comments and helpful discussions throughout the project; F. Wang for generous support; T. Machado for helpful comments on the manuscript; D. Goldstein for help with data analysis; and A. O'Neill-Dietel, G. Zhang, J. Golub, H. Kern, C. Jaycox, I. Bruckman and M. Wright-Moses for help with behavioural scoring. This work was funded by the Klingenstein Foundation (J.N.B.), the University of Pennsylvania School of Arts and Sciences (J.N.B.), the National Institutes of Health (F31DK131870 to N.G.), the National Science Foundation G.R.F.P. (N.G.) and the Blavatnik Family Foundation Fellowship (N.G.). J.N.B. is supported by the National Institutes of Health (1P01DK119130, 1R01DK133399, 1R01DK124801 and 1R01NS134976). A.M. is supported by the Simons Foundation. H.N.A. is supported by the National Institutes of Health (F32NS128392). T.S.N. is supported by the National Institutes of Health (K00NS124190) and an American Neuromuscular Foundation Development Grant. K.A.K. and M.K. are supported by the National Science Foundation G.R.F.P. N.K.S. is supported by the National Institutes of Health (F32DK135401 and T32DK731442). L.B. is supported by the American Heart Association (25POST1362884) and the Swiss National Science Foundation (206668). M.J.C. is supported by a Canadian Institutes of Health Research Project Grant (PJT-175156). R.K. is supported by the National Institutes of Health (RF1NS131165, R61NS126026 and R01NS120663). C.A.T. is supported by the National Institutes of Health (R01NS134976-02 and 1DP1DK140021-01). A.K. is supported by the National Institutes of Health (R00MH117264), the Simons Foundation, a McKnight Foundation Scholar Award and a Pew Biomedical Scholar Award.

Author contributions N.G. and J.N.B. initiated the project. N.G., H.N.A., T.S.N., K.A.K., M.K., J.R.E.C., L.B., E.L., R.E.V., E.C., E.L.M., M.A. and Y.D. performed and/or analysed in vivo or histological animal experiments. N.K.S. performed and analysed slice electrophysiology experiments. A.T.M.Y. and N.B. performed and analysed the spatial transcriptomics. M.J.C., R.K., C.A.T., B.K.T., A.K. and J.N.B. supervised the project. N.G. and J.N.B. created the figures and N.G., A.M., B.K.T., A.K. and J.N.B. wrote and revised the manuscript with input from all authors.

Competing interests The authors declare no competing interests.

Additional information

Supplementary information The online version contains supplementary material available at https://doi.org/10.1038/s41586-025-09602-x.

Correspondence and requests for materials should be addressed to Bradley K. Taylor, Ann Kennedy or J. Nicholas Betley.

Peer review information *Nature* thanks Ben Seymour and the other, anonymous, reviewer(s) for their contribution to the peer review of this work. Peer reviewer reports are available.

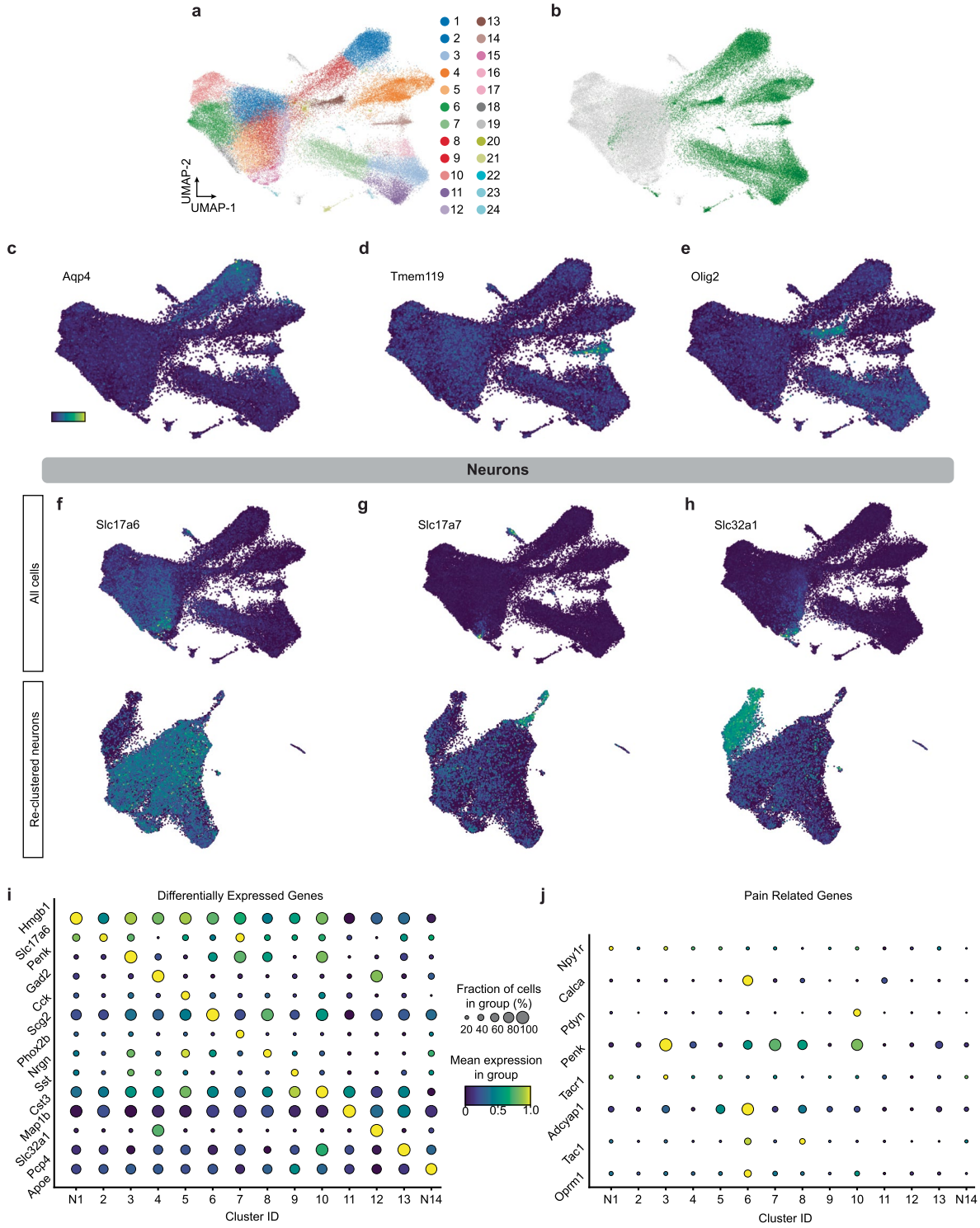

Extended Data Fig. 1 | See next page for caption.

Extended Data Fig. 1 | Transcriptomic analysis of PBN cells. (**a**) UMAP projection of all 76,201 PBN cells analyzed by spatial transcriptomics, with each cell colored by its assigned cluster. This clustering reflects only the transcriptional similarities. (**b**) UMAP embedding by glial identity. Cells expressing glial markers are shown in green. (**c**) UMAP embedding showing the normalized expression level of *Aqp4*, an astrocyte marker. Color scale maximum: 16. (**d**) UMAP embedding showing the normalized expression level of *Tmem119*, a microglia marker. Color scale maximum: 10. (**e**) UMAP embedding showing the normalized expression level of *Olig2*, an oligodendrocyte marker. Color scale maximum: 11. (**f**) (top) UMAP embedding showing the normalized expression level of *Slc17a6*, the gene encoding VGLUT2 as a marker of excitatory neurons in all PBN cells. Color scale maximum: 15. (bottom) UMAP embedding in re-clustered neurons showing the normalized expression level of *Slc17a6*. Color scale maximum: 2.35. (**g**) (top) UMAP embedding showing the normalized expression level of *Slc17a7*, the gene encoding VGLUT1 as a marker of excitatory neurons in all PBN cells. Color scale maximum: 51. (bottom) UMAP embedding in re-clustered neurons showing normalized the expression level of *Slc17a7*. Color scale maximum: 2.35. (**h**) (top) UMAP embedding showing the normalized expression level of *Slc32a1*, the gene encoding VGAT as a marker of inhibitory neurons in all PBN cells. Color scale maximum: 69. (bottom) UMAP embedding in re-clustered neurons showing the normalized expression level of *Slc32a1*. Color scale maximum: 3.15. (**i**) Dot plot showing a differentially expressed gene from each neuronal cluster. The size of the dot represents the number of cells within that cluster expressing the gene and the color of the dot represents the mean expression of that gene. (**j**) Dot plot showing the expression of genes previously identified as markers for populations of neurons that are involved in pain behaviors across each neuronal cluster.

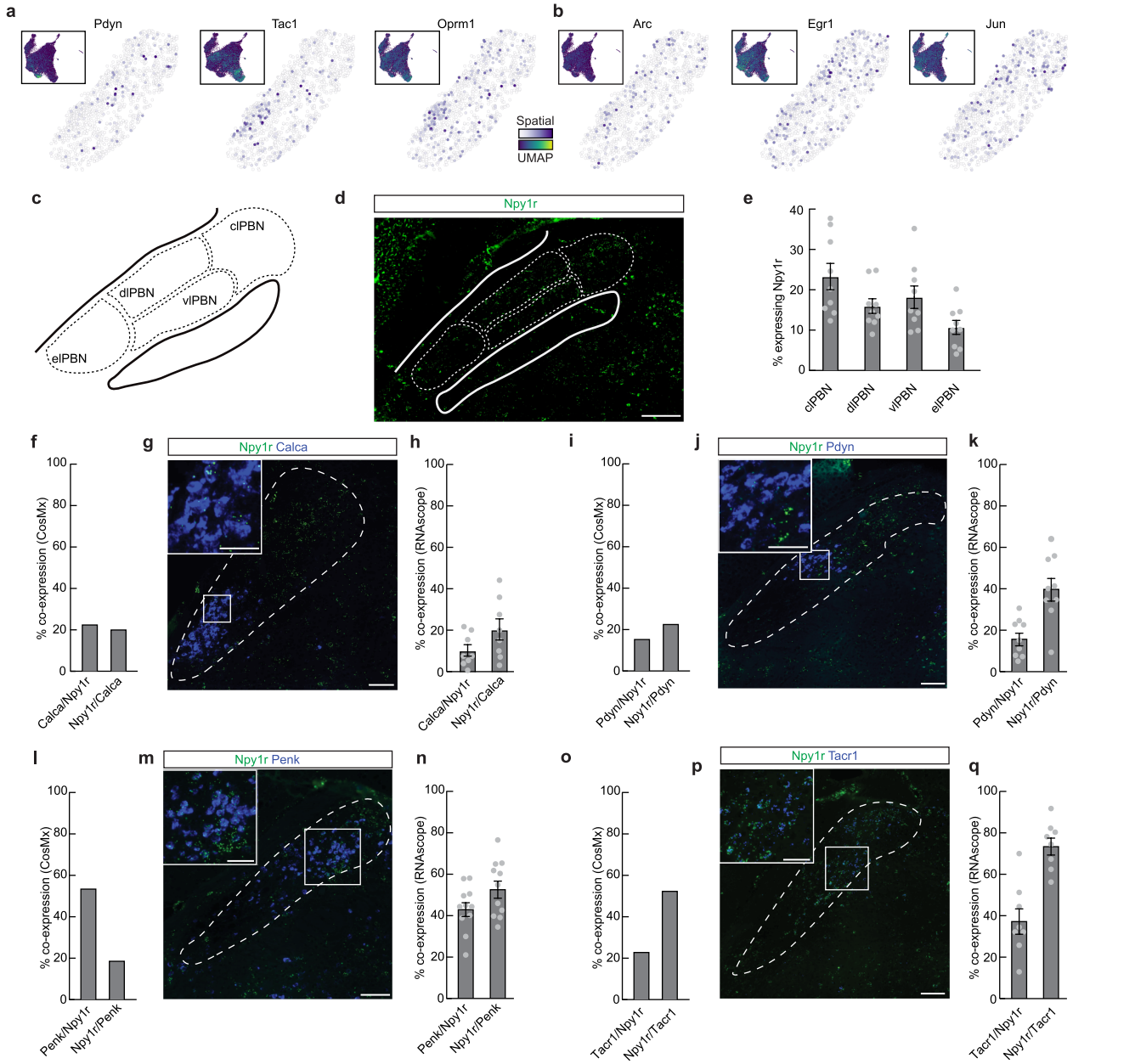

Extended Data Fig. 2 | Y1R co-expression with previously identified pain-related neuron populations in the PBN. (**a**) UMAP embedding and representative spatial maps showing normalized expression levels of *Pdyn*, *Tac1*, and *Oprm1*. UMAP scale maximum: Pdyn, 2.7; Tac1, 2.55; Oprm1, 2.3. Spatial scale maximum: Pdyn, 1.9; Tac1, 1.9; Oprm1, 1.8. (**b**) UMAP embedding and representative spatial maps showing normalized expression levels of the IEGs *Arc*, *Egr1*, and *Jun*. UMAP scale maximum: Arc, 3; Egr1, 2.4; Jun, 2.75. Spatial scale maximum: Arc, 1.75; Egr1, 2; Jun, 2. (**c**) Diagram depicting 4 subregions of the lPBN. (**d**) Representative image showing RNAscope fluorescence in situ hybridization (FISH) used to validate CosMx results. *Npy1r* expression was observed throughout the PBN. Scale bar, 200 µm. (**e**) % of neurons expressing *Npy1r* in each subregions of the lPBN. Each dot represents one section (n = 3 mice). (**f**) Overlap between *Calca* and *Npy1r* expression from CosMx analysis. (**g**) Representative image showing *Calca* and *Npy1r* in the lPBN labeled using RNAscope FISH. Scale bar, 100 µm; inset, 50 µm. (**h**) % of *Npy1r*-expressing neurons co-expressing *Calca* and % of *Calca*-expressing neurons co-expressing *Npy1r*. Each dot represents one section (n = 3 mice). (**i**) Overlap between *Pdyn* and *Npy1r* expression from CosMx analysis. (**j**) Representative image showing *Pdyn* and *Npy1r* in the lPBN labeled using RNAscope FISH. Scale bar, 100 µm; inset, 50 µm. (**k**) % of *Npy1r*-expressing neurons co-expressing *Pdyn* and % of *Pdyn*-expressing neurons co-expressing *Npy1r*. Each dot represents one section (n = 3 mice). (**l**) Overlap between *Penk* and *Npy1r* expression from CosMx analysis. (**m**) Representative image showing *Penk* and *Npy1r* in the lPBN labeled using RNAscope FISH. Scale bar, 100 µm; inset, 50 µm. (**n**) % of *Npy1r*-expressing neurons co-expressing *Penk* and % of *Penk*-expressing neurons co-expressing *Npy1r*. Each dot represents one section (n = 4 mice). (**o**) Overlap between *Tacr1* and *Npy1r* expression from CosMx analysis. (**p**) Representative image showing *Npy1r* and *Tacr1* in the lPBN labeled using RNAscope FISH. Scale bar, 100 µm; inset, 50 µm. (**q**) % of *Npy1r*-expressing neurons co-expressing *Tacr1* and % of *Tacr1*-expressing neurons co-expressing *Npy1r*. Each dot represents one section (n = 3 mice). Data are expressed as mean ± SEM.

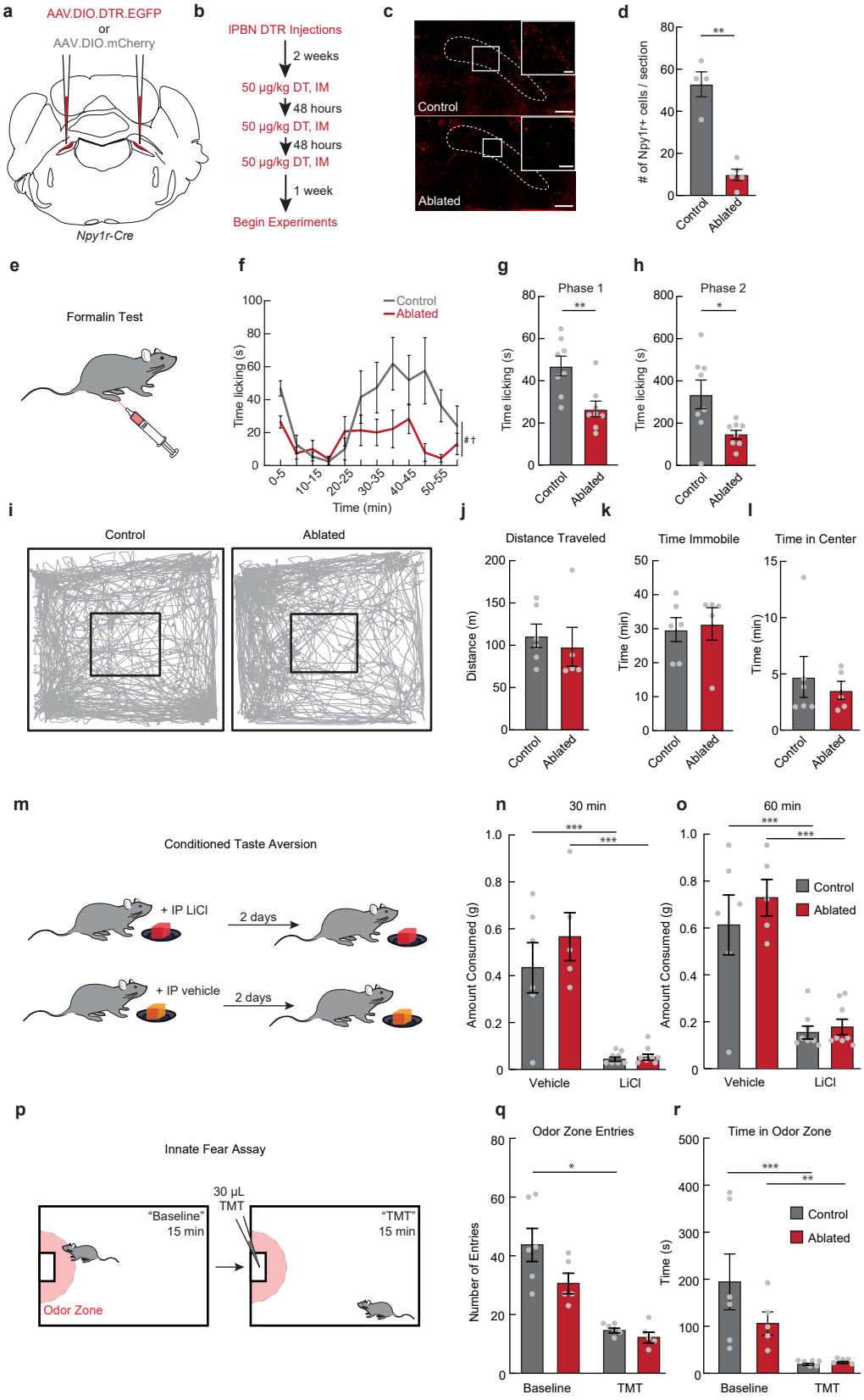

Extended Data Fig. 3 | See next page for caption.

Extended Data Fig. 3 | lPBN Y1R neuron ablation suppresses pain-related behaviors without affecting locomotion or responses to other negative stimuli. (**a**) Viral injection strategy for bilateral lPBN Y1R neuron ablation. (**b**) Experimental timeline for lPBN Y1R neuron ablation. (**c**) Representative images showing *Npy1r* mRNA in the lPBN labeled using RNAscope fluorescence in situ hybridization from a control and DTR-expressing mouse. Scale bar, 200 µm; insets, 50 µm. (**d**) Number of cells / section expressing *Npy1r* in the lPBN in control (n = 4) and ablated (n = 5) mice (unpaired two-sided t-test, p = 0.0023). (**e**) The formalin test was used to test the effect of lPBN Y1R neuron ablation on pain behavior. (**f**) Time spent licking paw in 5 min bins after an injection of formalin in control or Y1R ablated mice (n = 8 mice/group, two-way ANOVA, main effect of group p = 0.0205, group x time interaction p = 0.0217). (**g**) Time spent licking paw during phase 1 in (f) (n = 8 mice/group, unpaired t-test, p = 0.0042). (**h**) Time spent licking paw during phase 2 in (f) (n = 8 mice/group, unpaired t-test, p = 0.03). (**i**) Representative plots showing locomotion of control and ablated mice. (**j-l**) Distance traveled (**j**), time spent immobile (**k**), and time spent in the center of the arena (**l**) in control (n = 6) and ablated (n = 5) mice (unpaired t-tests, n.s.). (**m**) Conditioned taste aversion paradigm. (**n-o**) Amount of gel paired with saline or LiCl consumed by control and Y1R-ablated mice after 30 min (**n**) and 60 mins (**o**) (n = 6 control vehicle, n = 5 control ablated, n = 8 LiCl mice, two-way ANOVA, main effect of virus n.s.). (**p**) Predator odor avoidance paradigm. (**q**) Number of entries into the odor zone before and after addition of TMT in control (n = 6) and Y1R-ablated (n = 5) mice (two-way ANOVA, main effect of virus n.s.). (**r**) Time spent in the odor zone before and after addition of TMT in control (n = 6) and Y1R-ablated (n = 5) mice (two-way ANOVA, main effect of virus n.s.). Data are expressed as mean ± SEM. Grey dots represent individual mice. T-test and post-hoc comparisons: $^{*}p < 0.05$, $^{**}p < 0.01$, $^{***}p < 0.001$. ANOVA main effect of group: $^{\#}p < 0.05$. ANOVA interaction: $^{\dagger}p < 0.05$.

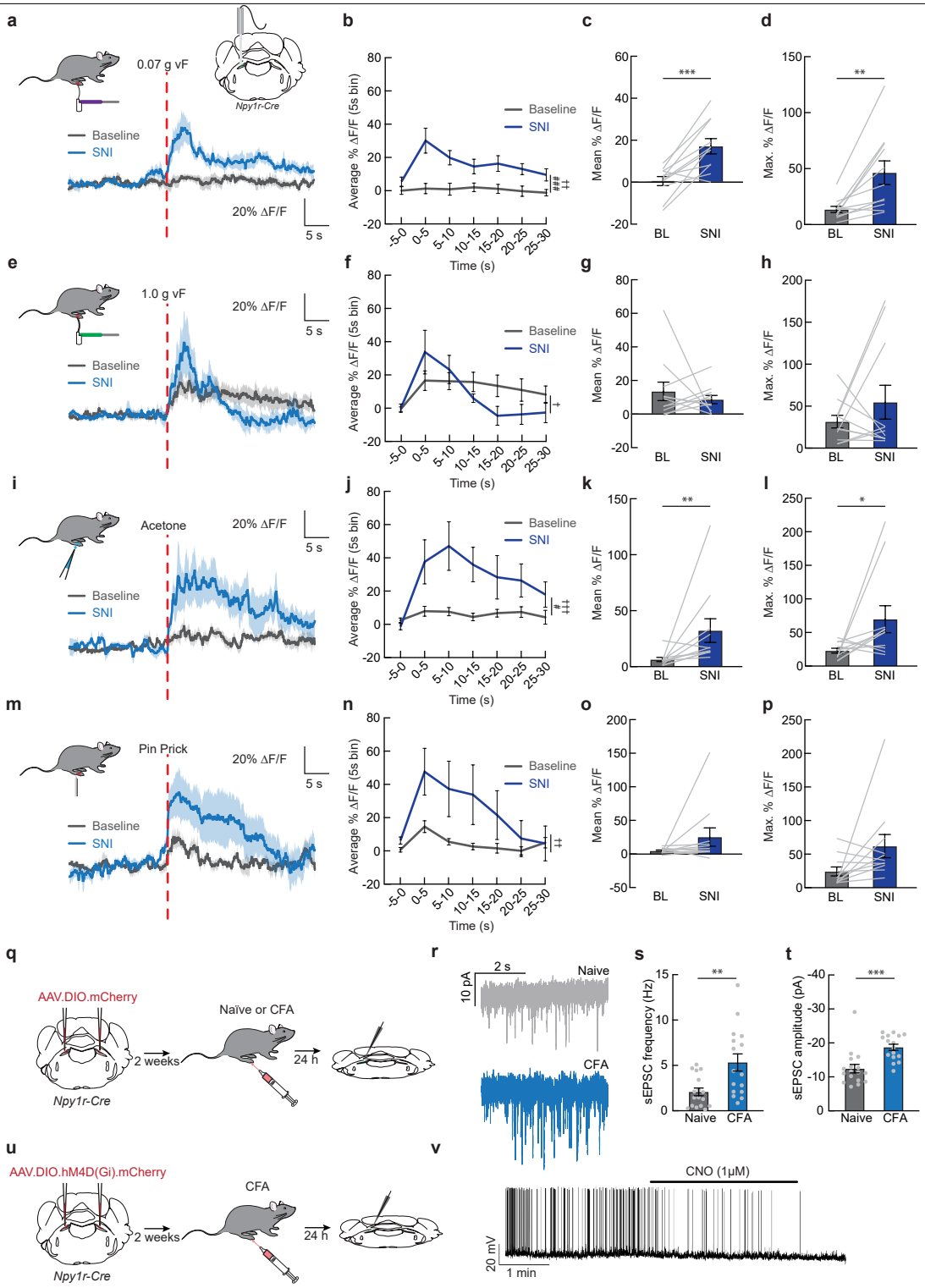

Extended Data Fig. 4 | See next page for caption.

Extended Data Fig. 4 | Injury sensitizes lPBN Y1R neurons. (**a**) ΔF/F of GCaMP6s signal from lPBN Y1R neurons during paw stimulation with a 0.07 g von Frey filament before and after SNI. Dark lines represent mean and lighter, shaded areas represent SEM. (**b**) Average ΔF/F (5 s bins) of the GCaMP6s signal shown in (a) (n = 11 mice, repeated measures two-way ANOVA, main effect of SNI p = 0.0009, SNI x time interaction p = 0.0046). (**c**-**d**) Mean (**c**) and maximum (**d**) ΔF/F of the GCaMP6s signal after the stimulus shown in (a) (n = 11 mice, paired two-sided t-test, p = 0.0008 (c), p = 0.0044 (d)) (**e**) ΔF/F of GCaMP6s signal from lPBN Y1R neurons during paw stimulation with a 1.0 g von Frey filament before and after SNI. (**f**) Average ΔF/F (5 s bins) of the GCaMP6s signal shown in (e) (n = 11 mice, repeated measures two-way ANOVA, SNI x time interaction p = 0.0239). (**g**-**h**) Mean (**g**) and maximum (**h**) ΔF/F of the GCaMP6s signal after the stimulus shown in (e) (n = 11 mice, two-sided Wilcoxon matched pairs signed-rank test, n.s. (g), paired two-sided t-test, n.s. (h)) (**i**) ΔF/F of GCaMP6s signal from lPBN Y1R neurons during paw stimulation with a cold stimulus (acetone) before and after SNI. (**j**) Average ΔF/F (5 s bins) of the GCaMP6s signal shown in (i) (n = 11 mice, repeated measures two-way ANOVA, main effect of SNI p = 0.0294, SNI x time interaction p = 0.0008). (**k**-**l**) Mean (**k**) and maximum (**l**) ΔF/F of the GCaMP6s signal after the stimulus shown in (i) (n = 11 mice, two-sided Wilcoxon matched pairs signed-rank test, p = 0.0049 (k), p = 0.0322 (l)) (**m**) ΔF/F of GCaMP6s signal from lPBN Y1R neurons during paw pin prick before and after SNI. (**n**) Average ΔF/F (5 s bins) of the GCaMP6s signal shown in (m) (n = 11 mice, repeated measures two-way ANOVA, SNI x time interaction p = 0.0015). (**o**-**p**) Mean (**o**) and maximum (**p**) ΔF/F of the GCaMP6s signal after the stimulus shown in (m) (n = 11 mice, two-sided Wilcoxon matched pairs signed-rank test, n.s.) (**q**) *Npy1r*-Cre mice were injected with a Cre-dependent fluorophore to label lPBN Y1R neurons. Mice were then injected with CFA and acute brain slices were prepared 24 h later. (**r**) Example traces from a whole-cell voltage clamp recording from an lPBN Y1R neuron from a naïve mouse (top, grey) and a mouse 24 h after a paw CFA injection (bottom, blue). (**s**-**t**) sEPSC frequency (**c**) and amplitude (**d**) in cells from naïve mice or mice 24 h after CFA injection (n = 16–17/group, unpaired t-test, p < 0.01 (c), p < 0.001 (d)). (**u**) *Npy1r*-Cre mice were injected with a Cre-dependent inhibitory DREADD that also expresses mCherry to label lPBN Y1R neurons. (**v**) Representative trace showing a decrease in firing of an lPBN Y1R neuron after bath application of the DREADD ligand CNO (1μM). Data are expressed as mean ± SEM. Grey dots and lines represent individual mice (a-p) or cells (s,t). BL, baseline. T-test and post-hoc comparisons: $^{*}p < 0.05$, $^{**}p < 0.01$, $^{***}p < 0.001$. ANOVA main effect of group: $^{\#}p < 0.05$, $^{\#\#\#}p < 0.001$. ANOVA interaction: $^{\dagger}p < 0.05$, $^{\dagger\dagger}p < 0.01$, $^{\dagger\dagger\dagger}p < 0.001$.

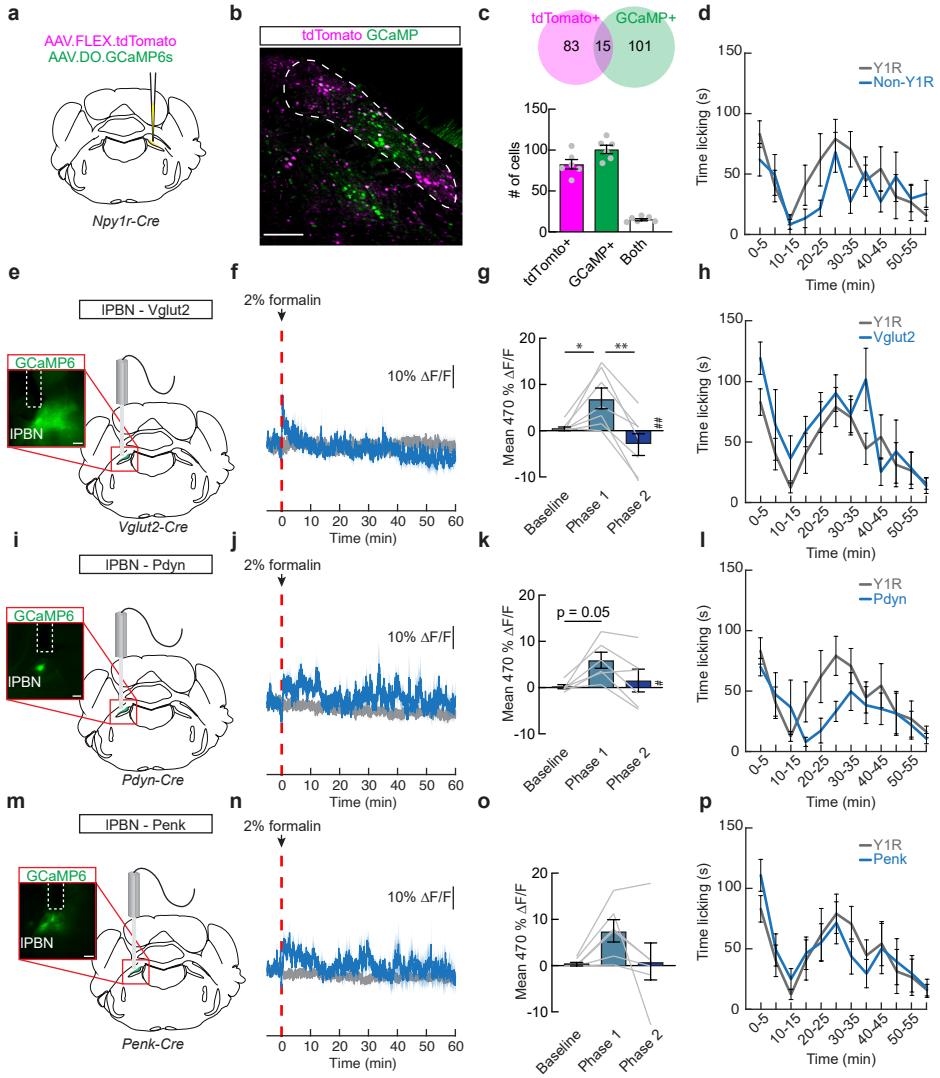

Extended Data Fig. 5 | Non-Y1R lPBN neurons do not exhibit tonic neural activity responses after formalin. (**a**) Injection strategy to confirm specificity of Cre-Off GCaMP (AAV.DO.GCaMP6s) expression in an *Npy1r*-Cre mouse. (**b**) Representative image showing Cre-Off GCaMP and Cre-dependent tdTomato expression in the PBN. Scale bar, 200 µm. (**c**) (top) Number of cells expressing only tdTomato, only GCaMP, or both in the PBN. (bottom) Average number of neurons expressing tdTomato, GCaMP, and both. Grey dots represent individual sections. (**d**) Time spent licking paw (5 min bins) after an injection of formalin while recording from Y1R or non-Y1R neurons (n = 9 Y1R, n = 6 non-Y1R mice, two-way ANOVA, n.s.) (**e**) Measuring calcium dynamics of lPBN *Vglut2*-expressing neurons. Inset, representative image showing GCaMP6s expression in lPBN Vglut2 neurons below a fiber optic track. Scale bar, 200 µm. (**f**) Average ΔF/F of GCaMP6s signal from lPBN Vglut2 neurons after a formalin injection. Blue, 470 nm; grey, 405 nm. Dark lines represent mean and lighter, shaded areas represent SEM. (**g**) Mean ΔF/F of lPBN Vglut2 neurons (n = 7 mice, one-way ANOVA, p = 0.0031). (**h**) Time spent licking paw (5 min bins) after an injection of formalin while recording from Y1R neurons or Vglut2 neurons (n = 9 Y1R, n = 7 Vglut2 mice, two-way ANOVA, n.s.). (**i**) Fiber photometry was used to measure calcium dynamics of lPBN *Pdyn*-expressing neurons. Inset, representative image showing GCaMP6s expression in lPBN Pdyn neurons below a fiber optic track. Scale bar, 200 µm. (**j**) Average ΔF/F of GCaMP6s signal from lPBN Pdyn neurons after a formalin injection. (**k**) Mean ΔF/F of lPBN Pdyn neurons (n = 6 mice, one-way ANOVA, $p < 0.05$). (**l**) Time spent licking paw (5 min bins) after an injection of formalin while recording from Y1R neurons or Pdyn neurons (n = 9 Y1R, n = 6 Pdyn mice, two-way ANOVA, n.s.). (**m**) Measuring calcium dynamics of lPBN *Penk*-expressing neurons. Inset, representative image showing GCaMP6s expression in lPBN Penk neurons below a fiber optic track. Scale bar, 200 µm. (**n**) Average ΔF/F of GCaMP6s signal from lPBN Penk neurons after a formalin injection. (**o**) Mean ΔF/F of lPBN Penk neurons (n = 6 mice, repeated measures one-way ANOVA, n.s.). (**p**) Time spent licking paw (5 min bins) after an injection of formalin while recording from Y1R neurons or Penk neurons (n = 9 Y1R, n = 6 Penk mice, two-way ANOVA, n.s.). Data are expressed as mean ± SEM. Grey lines represent individual mice. Post-hoc comparisons: $^{*}p < 0.05$. $^{**}p < 0.01$. ANOVA main effect of group: $^{\#}p < 0.05$, $^{\#\#}p < 0.01$.

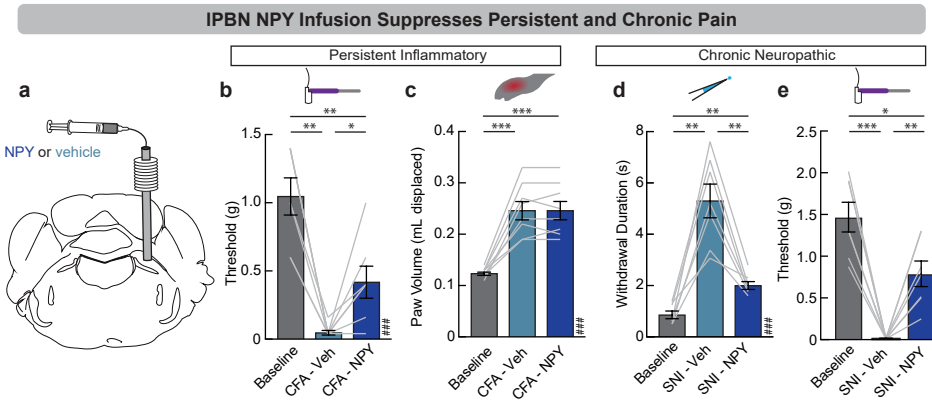

Extended Data Fig. 6 | lPBN infusion of NPY suppresses persistent inflammatory and chronic pain. (**a**) Neuropeptide Y (NPY) or vehicle was infused into the lPBN. Withdrawal thresholds were subsequently tested in animals with persistent inflammation from an injection of Complete Freund's Adjuvant (CFA) in the paw or SNI-induced neuropathy. (**b**) Withdrawal threshold to mechanical stimuli before CFA (baseline) and after CFA with a vehicle or NPY infusion (n = 7 mice, one-way ANOVA, $p < 0.001$). (**c**) Paw volume before CFA injection (baseline) and after CFA with a vehicle or NPY infusion (n = 8 mice, one-way ANOVA, $p < 0.001$). (**d-e**) Withdrawal threshold to a cold stimulus (**d**, acetone) or mechanical stimuli (**e**) before SNI (baseline) and after SNI with a vehicle or NPY infusion (n = 7 mice, one-way ANOVA, $p < 0.001$). Data are expressed as mean ± SEM. Grey lines represent individual mice. Post-hoc comparisons: $^{*}p < 0.05$, $^{**}p < 0.01$, $^{***}p < 0.001$. ANOVA main effect of group: $^{###}p < 0.001$.

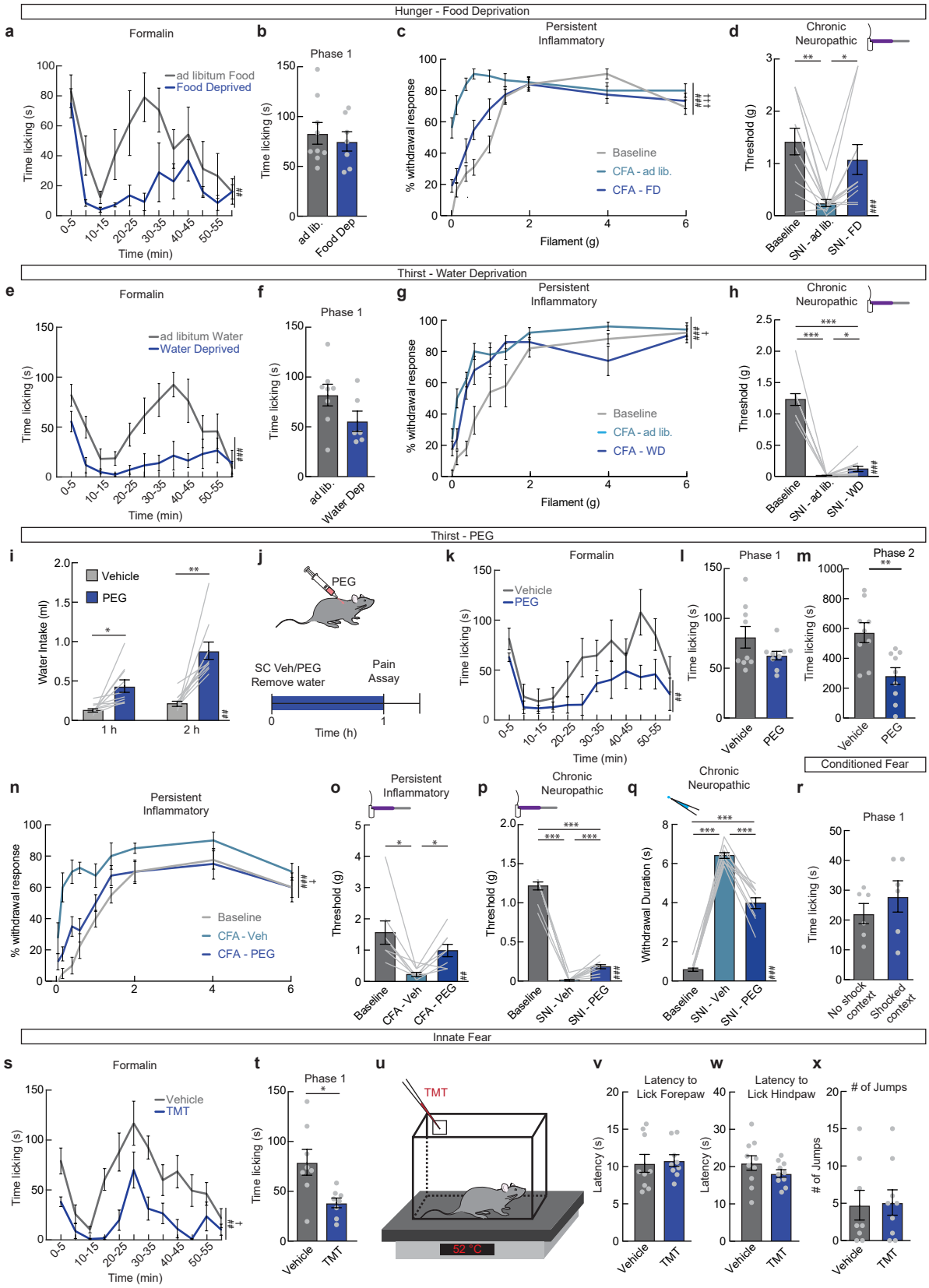

Extended Data Fig. 7 | See next page for caption.

Extended Data Fig. 7 | Competing needs suppress persistent pain, but not acute pain. (**a**) Time spent licking paw (5 min bins) after an injection of formalin in *ad libitum*-fed (n = 9) or 24 h food-deprived (n = 7) mice (two-way ANOVA, main effect of group p = 0.0031). (**b**) Time spent licking paw during phase 1 (n = 9 ad lib, n = 7 FD mice, unpaired two-sided t-test, n.s.). (**c**) Percent of trials where a paw withdrawal was observed after mechanical stimulation with a von Frey filament before CFA and after CFA in *ad libitum*-fed or food-deprived mice. Each von Frey filament was applied 5 times (n = 15 mice, two-way ANOVA, main effect of group p < 0.001, group x filament interaction p < 0.001). (**d**) Withdrawal threshold before SNI and after SNI in *ad libitum*-fed or food-deprived mice (n = 11 mice, one-way ANOVA, p = 0.0008). (**e**) Time spent licking paw (5 min bins) after an injection of formalin in mice with *ad libitum* access to water (n = 8) or 24 h water-deprived mice (n = 6) (two-way ANOVA, main effect of group p < 0.001). (**f**) Time spent licking paw during phase 1 (n = 8 ad lib, n = 6 WD mice, unpaired two-sided t-test, n.s.). (**g**) Percent of trials where a paw withdrawal was observed after mechanical stimulation with a von Frey filament before CFA and after CFA in mice with *ad libitum* access to water or water-deprived mice (n = 10 mice, two-way ANOVA, main effect of group p = 0.0005, group x filament interaction p = 0.0434). (**h**) Withdrawal threshold before SNI and after SNI in mice with *ad libitum* access to water or water-deprived mice (n = 11 mice, one-way ANOVA, p < 0.001). (**i**) Water intake 1 and 2 h after vehicle or PEG treatment (n = 10 mice, two-way ANOVA, main effect of group p = 0.0019). (**j**) Timeline of PEG experiments. (**k**) Time spent licking paw (5 min bins) after vehicle or PEG administration (n = 9 mice/group, two-way ANOVA, main effect of group p = 0.003). (**l**) Time spent licking during phase 1 (n = 9 mice/group, unpaired two-sided t-test, n.s.). (**m**) Time spent licking during phase 2 (n = 9 mice/group, unpaired two-sided t-test, p = 0.0043). (**n**) Percent of trials where a paw withdrawal was observed after stimulation with a von Frey filament before CFA and after CFA in vehicle- or PEG-treated mice (n = 8 mice, two-way ANOVA, main effect of group p < 0.001, group x filament interaction p = 0.0235). (**o**) Withdrawal threshold before CFA and after CFA in vehicle- or PEG-treated mice (n = 8 mice, one-way ANOVA, p = 0.0088). (**p**) Withdrawal threshold before SNI and after SNI in vehicle- or PEG-treated mice (n = 10 mice, one-way ANOVA, p < 0.001). (**q**) Withdrawal duration after acetone administration before SNI and after SNI in vehicle- or PEG-treated mice (n = 10 mice, one-way ANOVA, p < 0.001). (**r**) The effect of conditioned fear on phase 1 of the response to formalin-induced pain (n = 6 mice/group, unpaired two-sided t-test, n.s.) (**s**) Time spent licking paw (5 min bins) with control PBS or TMT in the chamber (n = 8 mice/group, two-way ANOVA, main effect of group p = 0.001, group x time interaction p = 0.0307). (**t**) Time spent licking paw during phase 1 (n = 8 mice/group, unpaired two-sided t-test, p = 0.0162). (**u**) TMT was applied to a chamber placed on 52 °C hot plate. Mice were then placed in the chamber and their behavior was recorded for 1 min. (**v-x**) Latency to lick the forepaw (**v**) and hind paw (**w**) and the number of jumps (**x**) on the hot plate after application vehicle or TMT (n = 9 mice/group (v), n = 10 mice/group (w), n = 8 veh, n = 9 TMT mice (x) unpaired two-sided t-tests, all n.s.). Data are expressed as mean ± SEM. Grey dots and lines represent individual mice. T-test and post-hoc comparisons: $^{*}p < 0.05$, $^{**}p < 0.01$, $^{***}p < 0.001$. ANOVA main effect of group: $^{\#\#}p < 0.01$, $^{\#\#\#}p < 0.001$. ANOVA interaction: $^{\dagger}p < 0.05$, $^{\dagger\dagger\dagger}p < 0.001$.

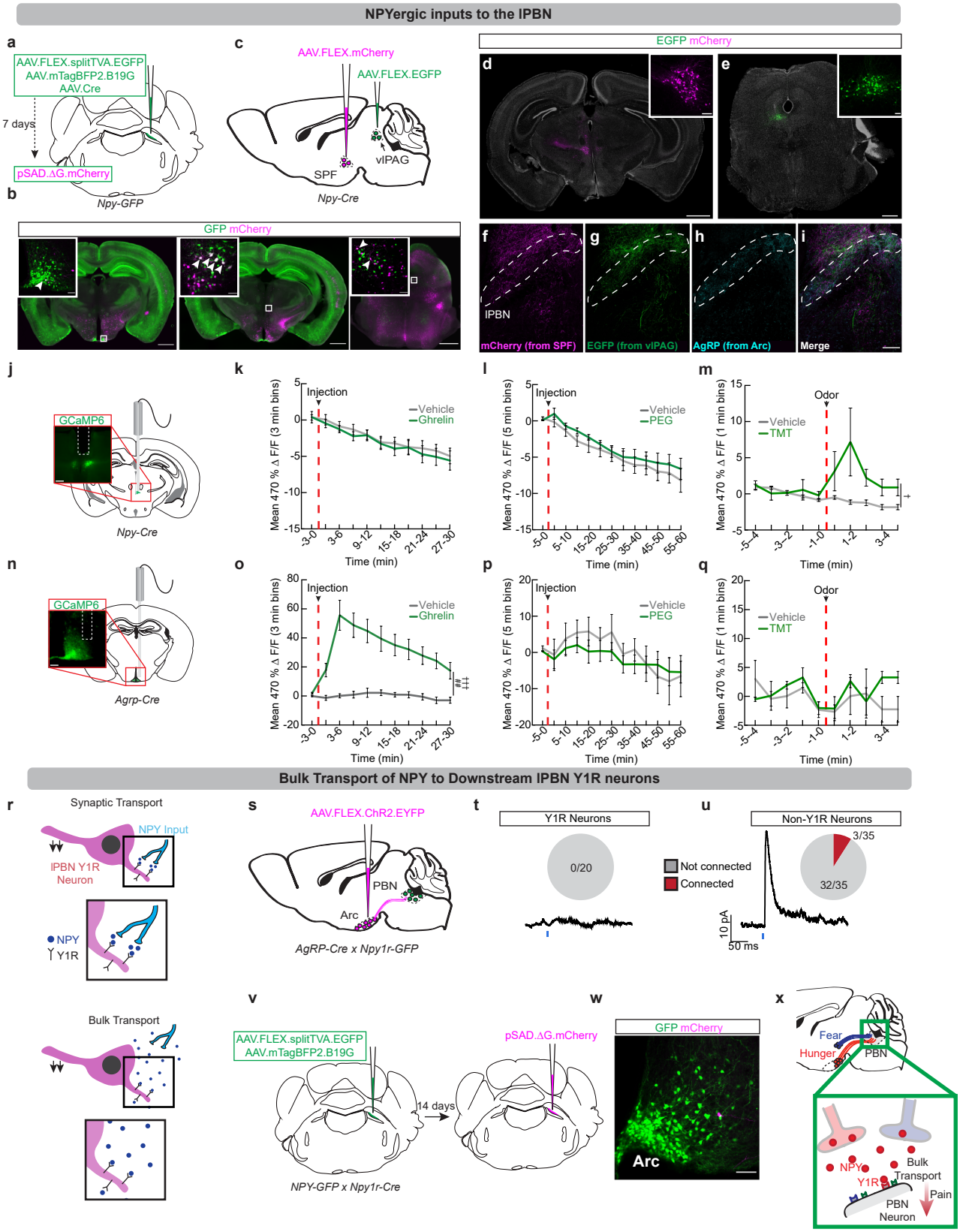

Extended Data Fig. 8 | See next page for caption.

Extended Data Fig. 8 | NPYergic inputs to the lPBN activated by competing survival threats. (**a**) Monosynaptic rabies tracing was performed in *Npy*-GFP mice to identify *Npy*-expressing inputs to the lPBN. (**b**) Three regions containing double-labeled *Npy*-positive (GFP) and rabies-positive (mCherry) neurons. Left, arcuate nucleus; middle, subparafascicular nucleus; right, ventrolateral periaqueductal grey. Scale bar, 1 mm (inset, 50 µm). (**c**) Labeling strategy to map NPY axon inputs to the lPBN. To visualize NPY inputs from the arcuate nucleus, post-hoc immunohistochemistry to AgRP[75] was used. (**d-e**) Representative image showing mCherry expression in SPF (**d**) and GFP expression in vlPAG (**e**) NPY neurons. Grey, DAPI. Scale bar, 1 mm (inset, 100 µm) (**f-i**) Representative image showing axons from the SPF (**f**), vlPAG (**g**) and arcuate nucleus (**h**) and a merged image showing the overlap (**i**). Scale bar, 100 µm. (**j**) Fiber photometry was used to record activity of SPF *Npy*-expressing neurons. Inset, representative image showing GCaMP6s expression in SPF NPY neurons below the fiber optic track. Scale bar, 200 µm. (**k**) Mean ΔF/F in 3 min bins of GCaMP6s signal in SPF NPY neurons after an injection of vehicle or ghrelin (600 µg/kg, n = 5 mice, two-way ANOVA, n.s.). (**l**) Mean ΔF/F in 5 min bins of GCaMP6s signal in SPF NPY neurons after an injection of vehicle or PEG (n = 5 mice, two-way ANOVA, n.s.). (**m**) Mean ΔF/F in 1 min bins of GCaMP6s signal in SPF NPY neurons after vehicle or TMT exposure (n = 5 mice, two-way ANOVA, main effect of group $p = 0.05$, group x time interaction $p = 0.0288$). (**n**) Fiber photometry was used to record activity of arcuate nucleus *Agrp*/*Npy*-expressing neurons. Inset, representative image showing GCaMP6s expression in arcuate NPY neurons below a fiber optic track. Scale bar, 200 µm. (**o**) Mean ΔF/F in 3 min bins of GCaMP6s signal in arcuate NPY neurons after an injection of vehicle (n = 6 mice) or 600 µg/kg ghrelin (n = 15 mice, two-way ANOVA, main effect of group $p = 0.0044$, group x time interaction $p < 0.001$). (**p**) Mean ΔF/F in 5 min bins of GCaMP6s signal in arcuate NPY neurons after an injection of vehicle or PEG (n = 4 mice, two-way ANOVA, n.s.). (**q**) Mean ΔF/F in 1 min bins of GCaMP6s signal in arcuate NPY neurons after vehicle (n = 5 mice) or TMT exposure (n = 4 mice, two-way ANOVA, n.s.). (**r**) Two possible NPY signaling mechanisms. (**s**) Channelrhodopsin-assisted circuit mapping – activation of arcuate NPY projections to the lPBN while monitoring activity in lPBN Y1R neurons. (**t**) Representative trace showing a lack of evoked current in an lPBN Y1R neuron following activation of NPY inputs. None of the 20 patched neurons showed inhibitory post synaptic currents (IPSC, n = 3 mice). (**u**) Representative trace of an evoked IPSC in a non-lPBN neuron following activation of NPY inputs (blue). 3/35 neurons patched showed inhibitory post synaptic potentials (n = 3 mice). (**v**) Monosynaptic rabies tracing was performed from lPBN Y1R neurons to determine whether arcuate NPY neurons form synaptic connections. (**w**) Representative image of arcuate NPY neurons and rabies-expressing presynaptic inputs. Scale bar, 200 µm. (**x**) Summary schematic. Data are expressed as mean ± SEM. ANOVA main effect of group: $^{\#\#}p < 0.01$. ANOVA interaction: $^{\dagger}p < 0.05$, $^{\dagger\dagger\dagger}p < 0.001$.

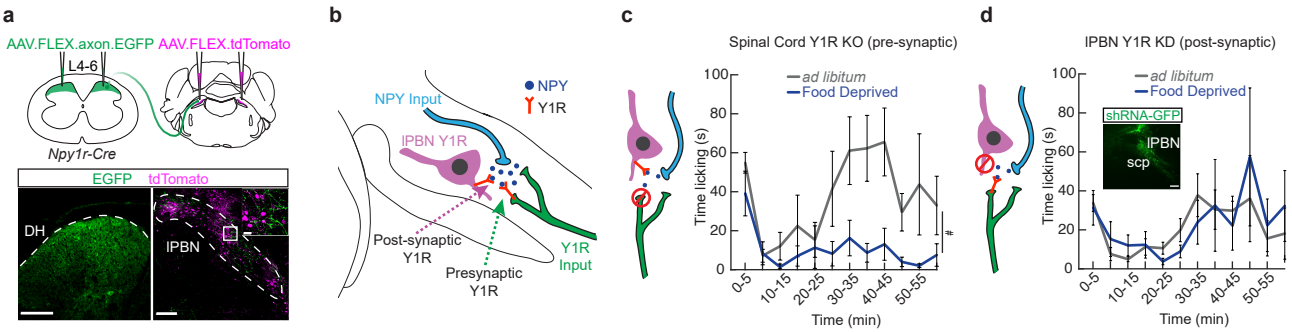

Extended Data Fig. 9 | Hunger suppresses inflammatory pain by acting on Y1 receptors on lPBN neurons. (**a**) (Top) Cre-dependent axon-enriched EGFP was injected in the dorsal horn and Cre-dependent tdTomato was injected into the lPBN of *Npy1r*-Cre mice to visualize neurons that express *Npy1r* and thus are potential pre- and post-synaptic sites of action of NPY in the lPBN. (Bottom) Representative images showing Y1R neurons expressing EGFP at the site of injection in the dorsal horn (left) and their projections to the lPBN along with lPBN Y1R neurons labeled with tdTomato (right). Scale bar, 200 µm (inset, 10 µm). (**b**) Diagram depicting two possible sites of action of NPY in the lPBN: presynaptic inputs from the spinal cord and postsynaptic receptors on lPBN neurons. (**c**) Y1 receptors were conditionally deleted from the spinal cord to reduce pre-synaptic signaling by crossing *Npy1r*-lox/lox mice with *Lbx1*-Cre mice[32]. Time spent licking paw in 5 min bins after an injection of formalin in *ad libitum*-fed and food-deprived mice (n = 6 mice, repeated measures two-way ANOVA, main effect of group p = 0.0144). (**d**) Y1 receptor expression was knocked down in the lPBN to reduce post-synaptic signaling by injecting an AAV expressing short hairpin RNA (shRNA) targeting the *Npy1r* gene. Inset shows shRNA-GFP expression in the lPBN. Scale bar, 200 µm. Time spent licking paw in 5 min bins after an injection of formalin in *ad libitum*-fed and food-deprived mice (n = 7 ad lib, n = 5 FD mice, repeated measures two-way ANOVA, n.s.). Data are expressed as mean ± SEM. ANOVA main effect of group: $^{\#}p < 0.05$.

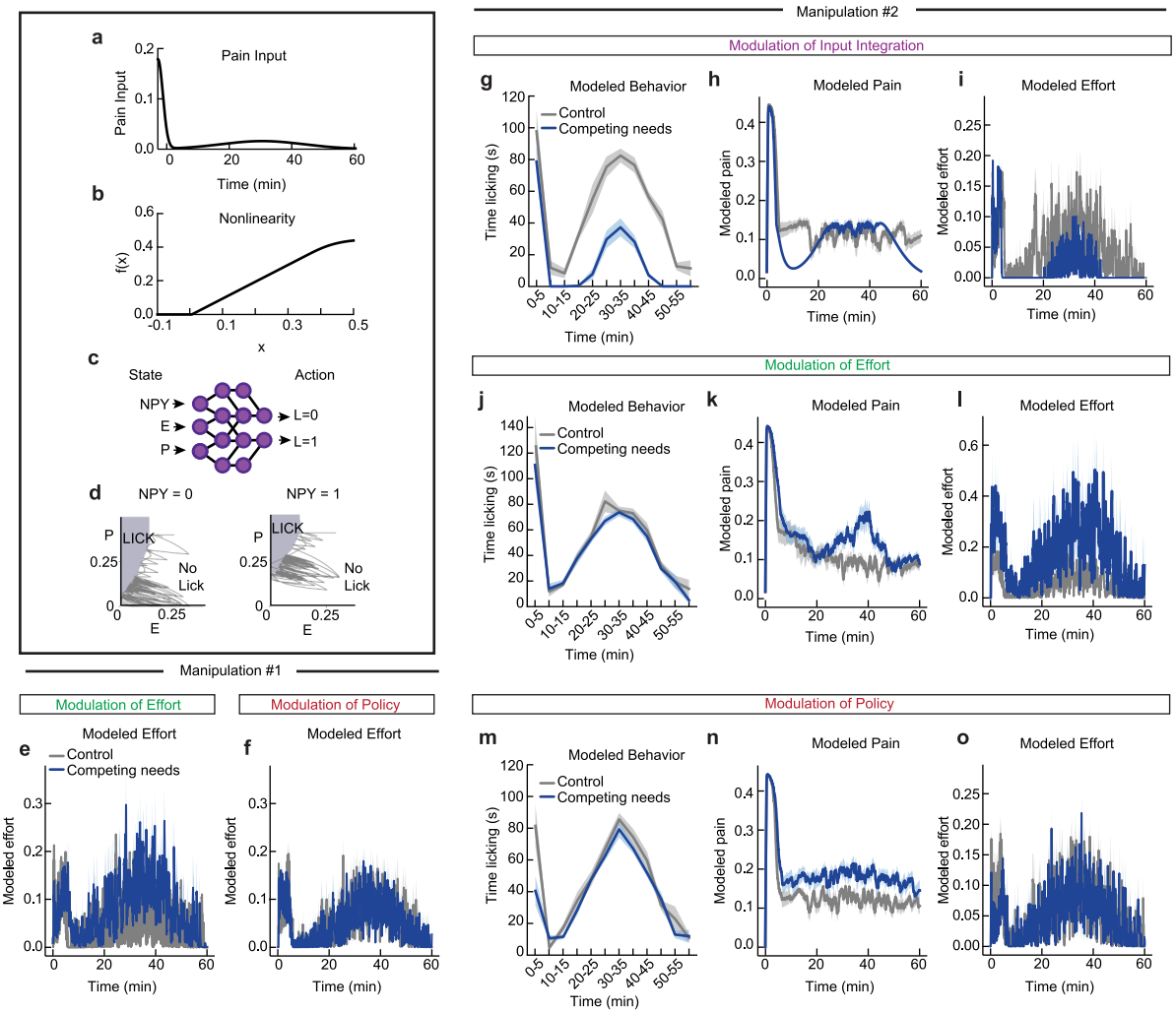

Extended Data Fig. 10 | Modeling pain behavior, pain state, and effort following formalin administration. (**a**) The average pain input given when training and simulating the model, chosen as the sum of two Gaussians corresponding to phases 1 and 2 of the formalin response. Model input during training and simulation is a noisy version of this input. (**b**) The pain state of the model is an integral of the pain input passed through a rectified saturating nonlinearity, shown here. (**c**) Schematic of the neural network implementing the behavioral policy, also showing the addition of a third state dimension 'NPY' that is 1 in the presence of a competing survival need and 0 otherwise (used in "Modulation of Policy" simulations). (**d**) Example policy space after training one model in the "Modulation of Policy" scenario in which the model learns a distinct policy for the presence vs absence of a competing need state. The dark gray line indicates a trajectory in the pain-effort state space, while the light gray region indicates the portion of pain-effort state space in which the model produces a lick response (no lick response is produced outside this region). When NPY = 1, the lick region shifts upwards compared to NPY = 0, corresponding to an increase in the pain threshold required to produce a licking response. (**e-f**) Average 'effort' dynamics of 8 trained models for the baseline model ('control') vs a model that increases the effort cost of licking (**e**) or introduces a third axis to the behavioral control policy (**f**). Dark lines represent mean and lighter, shaded areas represent SEM. (**g-o**) Simulation results using alternative formulations of input integration, effort modulation, and policy modulation (see equation 2 for each manipulation in the Methods). (**g-i**) Simulated licking behavior (g), 'pain' state (h) and 'effort' state (i) in the baseline condition ('control') vs a competing need that alters integration of nociceptive input using manipulation 2. (**j-l**) Simulated licking behavior (j), 'pain' state (k) and 'effort' state (l) in the baseline condition ('control') vs a competing need that alters the effort cost of licking using manipulation 2. (**m-o**) Simulated licking behavior (m), 'pain' state (n) and 'effort' state (o) in the baseline condition ('control') vs a competing need that adds a third dimension to the behavioral control policy using manipulation 2. Data are expressed as mean ± SEM.

nature portfolio

Corresponding author(s): J Nicholas Betley

Last updated by author(s): Jul 31, 2025

Reporting Summary

Nature Portfolio wishes to improve the reproducibility of the work that we publish. This form provides structure for consistency and transparency in reporting. For further information on Nature Portfolio policies, see our Editorial Policies and the Editorial Policy Checklist.

Statistics

For all statistical analyses, confirm that the following items are present in the figure legend, table legend, main text, or Methods section.

n/a	Confirmed	
☐	☒	The exact sample size (*n*) for each experimental group/condition, given as a discrete number and unit of measurement
☐	☒	A statement on whether measurements were taken from distinct samples or whether the same sample was measured repeatedly
☐	☒	The statistical test(s) used AND whether they are one- or two-sided *Only common tests should be described solely by name; describe more complex techniques in the Methods section.*
☐	☒	A description of all covariates tested
☐	☒	A description of any assumptions or corrections, such as tests of normality and adjustment for multiple comparisons
☐	☒	A full description of the statistical parameters including central tendency (e.g. means) or other basic estimates (e.g. regression coefficient) AND variation (e.g. standard deviation) or associated estimates of uncertainty (e.g. confidence intervals)
☐	☒	For null hypothesis testing, the test statistic (e.g. *F*, *t*, *r*) with confidence intervals, effect sizes, degrees of freedom and *P* value noted *Give P values as exact values whenever suitable.*
☒	☐	For Bayesian analysis, information on the choice of priors and Markov chain Monte Carlo settings
☒	☐	For hierarchical and complex designs, identification of the appropriate level for tests and full reporting of outcomes
☐	☒	Estimates of effect sizes (e.g. Cohen's *d*, Pearson's *r*), indicating how they were calculated

Our web collection on statistics for biologists contains articles on many of the points above.

Software and code

Policy information about availability of computer code

Data collection	CosMx (Nanostring) was used to collect spatial transcriptomics data. Synapse Neurophysiology Suite (Tucker Davis Technologies) was used to collect fiber photometry data. Miniscope Data Acquisition Software (UCLA) was used to acquire endoscopic imaging data. ANY-maze (Stoelting, v7.08) was used to collect open field and conditioned place preference data. Microscopy data was collected using LASX software (Leica, v3.7.4).
Data analysis	AtoMx Spatial Informatics Platform (Nanostring) and Python (v3.9.21) were used to analyze spatial transcriptomics data. Minian and MATLAB 2024b (Mathworks) were use to analyze endoscopic imaging data. Clampfit 11 was used to analyze slice physiology data. ANY-maze (Stoelting, v.7.08) was used to analyze freezing, open field, and place preference data. Microscopy data were analyzed using ImageJ (NIH, v1.53f). MATLAB and Prism 10 (GraphPad) were used to plot all other data and perform statistical analyses.

For manuscripts utilizing custom algorithms or software that are central to the research but not yet described in published literature, software must be made available to editors and reviewers. We strongly encourage code deposition in a community repository (e.g. GitHub). See the Nature Portfolio guidelines for submitting code & software for further information.

Data

Policy information about availability of data

All manuscripts must include a data availability statement. This statement should provide the following information, where applicable:

- Accession codes, unique identifiers, or web links for publicly available datasets
- A description of any restrictions on data availability
- For clinical datasets or third party data, please ensure that the statement adheres to our policy

Source data are provided with this paper. The spatial transcriptomic dataset generated in this study has been deposited in NCBI's Gene Expression Omnibus and are accessible through GEO Series accession number GSE301435 (https://www.ncbi.nlm.nih.gov/geo/query/acc.cgi?acc=GSE301435).

Research involving human participants, their data, or biological material

Policy information about studies with human participants or human data. See also policy information about sex, gender (identity/presentation), and sexual orientation and race, ethnicity and racism.

Reporting on sex and gender	N/A
Reporting on race, ethnicity, or other socially relevant groupings	N/A
Population characteristics	N/A
Recruitment	N/A
Ethics oversight	N/A

Note that full information on the approval of the study protocol must also be provided in the manuscript.

Field-specific reporting

Please select the one below that is the best fit for your research. If you are not sure, read the appropriate sections before making your selection.

☒ Life sciences ☐ Behavioural & social sciences ☐ Ecological, evolutionary & environmental sciences

For a reference copy of the document with all sections, see nature.com/documents/nr-reporting-summary-flat.pdf

Life sciences study design

All studies must disclose on these points even when the disclosure is negative.

Sample size	Sample sizes were chosen based on standards in the neuroscience field and variability in our prior data (Alhadeff et al., 2018; Alhadeff et al., 2019; Alhadeff et al., 2020; Goldstein et al., 2021; Klima et al., 2023). For anatomical experiments, at least 3 sections were analyzed from at least 3 mice per group. Neurophysiology data was sampled from at least 4 mice per group and behavioral experiments involved at least 5 mice per group.
Data exclusions	In Figure 1G, samples with fewer than 10 cells that met the criteria were excluded (Cluster N5 Npy1r+, 1 excluded; Cluster N8 Npy1r+, 6 excluded; Cluster N9 Npy1r+, 3 excluded; Cluster N10 Npy1r+, 2 excluded). Clusters N11-N14 were excluded due to low cell counts in both groups. Extended Data Figure 7V-X: one mouse from each group did not lick their forepaws during the assay and 2 PBS mice and one TMT mouse jumped onto the paper for several seconds and therefore their jump score was excluded. Extended Data Figure 8Q: one statistical outlier was identified in the TMT group using the ROUT method and was removed.
Replication	Results were successfully reproduced in all cases where multiple cohorts were used in the same experiment. At least two individuals scored behavioral assays and their results were averaged. A third scorer was used in cases where there was significant deviation between the two initial scorers.
Randomization	Mice were randomly assigned to experimental groups in between-subject analyses and experimental condition was randomized and counterbalanced in within-subject analyses. Cage-mate controls were used when possible (control groups for DREADD and ablation experiments, intracerebral infusions). Aged-matched cages were assigned to the same groups for water- and food-deprivation experiments. Males and females were randomly and approximately evenly assigned to experimental groups.
Blinding	In experiments where data were analyzed posthoc (formalin, hot plate, fiber photometry, miniscope) blinding was performed during data analysis only. In experiments where behavior was analyzed by investigators collecting the data (von Frey test, acetone test), blinding was performed prior to data collection.

Reporting for specific materials, systems and methods

We require information from authors about some types of materials, experimental systems and methods used in many studies. Here, indicate whether each material, system or method listed is relevant to your study. If you are not sure if a list item applies to your research, read the appropriate section before selecting a response.

Materials & experimental systems

n/a	Involved in the study
☐	☒ Antibodies
☒	☐ Eukaryotic cell lines
☒	☐ Palaeontology and archaeology
☐	☒ Animals and other organisms
☒	☐ Clinical data
☒	☐ Dual use research of concern
☒	☐ Plants

Methods

n/a	Involved in the study
☒	☐ ChIP-seq
☒	☐ Flow cytometry
☒	☐ MRI-based neuroimaging

Antibodies

Antibodies used

Goat anti-AgRP 1:2,500 (Neuromics GT15023)
Rabbit anti-cFos 1:1,500 (Cell Signaling Technology 2250)
Guinea Pig anti-RFP 1:10,000 (J. Nicholas Betley, UPenn; Betley et al., 2013)
Rabbit anti-GFP 1:5,000 (Invitrogen A-11122)
Donkey anti-Goat Cy5 AffiniPure 1:500 (Jackson ImmunoResearch 705-175-147)
Donkey anti-Rabbit Cy5 AffiniPure 1:500 (Jackson ImmunoResearch 711-175-152)
Donkey anti-Guinea Pig Cy3 AffiniPure 1:500 (Jackson ImmunoResearch 706-165-148)
Donkey anti-Rabbit Alexa Fluor 488 AffiniPure 1:500 (Jackson ImmunoResearch 711-545-152)

Validation

Primary antibodies were validated in previous studies.

AgRP - 4 citations: https://www.neuromics.com/agouti-related-protein-agrp-pubs-dia?srsltid=AfmBOopo_OKBckEOnVFDXwq8l4P0jdKIERbs0QTmrgYE6D1s0rCBVnQ6; 17 citations: https://www.citeab.com/antibodies/693182-af634-mouse-agrp-art-antibody?des=)

cFos - 1,119 citations: https://www.citeab.com/antibodies/123097-2250-c-fos-9f6-rabbit-mab?des=

RFP: Betley et al., 2013 https://doi.org/10.1016/j.cell.2013.11.002

GFP - 4,373 citations: https://www.citeab.com/antibodies/2401163-a-11122-gfp-polyclonal-antibody?des=

Animals and other research organisms

Policy information about studies involving animals; ARRIVE guidelines recommended for reporting animal research, and Sex and Gender in Research

Laboratory animals

Mice were group housed on a 12 h light/12 h dark cycle with ad libitum access to food and water unless otherwise noted. Temperature (21.5 to 22.3°C) and humidity (50 ± 15%) were controlled. Group housed adult male and female mice (at least 8 weeks old) were used for experimentation. The following strains were used:

Npy1r-Cre (Jackson Labs 030544, B6.Cg-Npy1rtm1.1(cre/GFP)Rpa/J, Npy-Flp (Jackson Labs 030211, B6.Cg-Npytm1.1(flpo)Hze/J), Pdyn-IRES-Cre (Jackson Labs 027958, B6;129S-Pdyntm1.1(cre)Mjkr/LowlJ), Penk-IRES2-Cre (Jackson Labs 025112, B6;129SPenktm2(cre)Hze/J), Vglut2-IRES-Cre (Jackson Labs 016963, Slc17a6tm2(cre)Lowl/J), Y1-lox/lox, Lbx1-Cre (Lbx1tm3.1(cre)Cbm), Npy-IRES-Cre (Jackson Labs 027851, B6.Cg-Npytm1(cre)Zman/J), Agrp-IRES-Cre (Jackson Labs 012899, Agrptm1(cre)Lowl/J), NPY-hrGFP (Jackson Labs 006417, B6.FVB-Tg(Npy-hrGFP)1Lowl/J), and C57BL/6J

Wild animals

This study did not involve wild animals.

Reporting on sex

Groups were composed of both male and female mice and sexes were combined in all analyses. We did not observe significant sex differences though sample sizes in some experiments did not allow for statistical comparison between sexes.

Field-collected samples

This study did not involve samples collected from the field.

Ethics oversight

All procedures were approved by the University of Pennsylvania, University of Florida, and University of Pittsburgh Institutional Animal Care and Use Committees

Note that full information on the approval of the study protocol must also be provided in the manuscript.

Plants

Seed stocks	N/A
Novel plant genotypes	N/A
Authentication	N/A